

# **Terahertz-metallization of NdNiO<sub>3</sub>**

Mattias Matthiesen

# Table of contents

<b>Preface</b>	<b>3</b>
<b>I Linear spectroscopy</b>	<b>4</b>
<b>1 Temperature</b>	<b>5</b>
1.1 Film . . . . .	5
1.2 Metasurface . . . . .	6
1.3 Calculations . . . . .	6
1.4 Metasurface with finite scattering time . . . . .	11
<b>2 Sample comparisons</b>	<b>16</b>
<b>3 Substrate</b>	<b>17</b>
<b>II Dynamics</b>	<b>20</b>
<b>4 Pump-probe overlap</b>	<b>21</b>
4.1 Experiment . . . . .	21
4.2 Calculations . . . . .	22
4.3 Mapping . . . . .	23
4.4 Scan type illustrations . . . . .	25
4.5 1D scan . . . . .	27
4.6 Rise and decay time scaling . . . . .	27
4.6.1 Field strength dependence . . . . .	27
4.6.2 Temperature dependence . . . . .	28
<b>5 Decay dynamics</b>	<b>30</b>
5.1 2D scans . . . . .	30
5.1.1 Second-order kinetics . . . . .	30
5.1.2 Power-law decay . . . . .	31
5.1.3 Multi-exponential decay, segregated . . . . .	32
5.1.4 Multi-exponential decay . . . . .	33
5.1.5 Paper plot . . . . .	34
5.2 One-dimensional scans . . . . .	34

<b>III Electric field susceptibility</b>	<b>39</b>
<b>6 Temperature</b>	<b>40</b>
6.1 Experiment . . . . .	40
6.2 Calculations . . . . .	41
6.3 Field-assisted tunneling . . . . .	44
<b>7 Nanosecond dynamics</b>	<b>47</b>
7.1 Experiment . . . . .	47
7.2 Calculations . . . . .	49
7.3 Extracting the resonator-gap conductivity $\sigma$ . . . . .	50
7.4 Timescales . . . . .	54
<b>8 Detailed look at three timescales</b>	<b>59</b>
8.1 Experiment . . . . .	59
8.2 Calculations . . . . .	61
8.3 Mapping . . . . .	61
<b>IV Photodoping</b>	<b>67</b>
<b>9 Photodoping a film</b>	<b>68</b>
9.1 Sample comparison . . . . .	73
<b>V Nonlinear spectroscopy</b>	<b>75</b>
<b>10 Comparing low and moderate temperature</b>	<b>76</b>
<b>VI Cavity</b>	<b>79</b>
<b>11 Field enhancement</b>	<b>80</b>
<b>12 Cavity polarization</b>	<b>87</b>

# Preface

This book details the analysis of measurements of NdNiO<sub>3</sub> thin films, coupled to an electro-magnetic metasurface consisting of golden electric split-ring resonators.

# **Part I**

## **Linear spectroscopy**

# 1 Temperature

## 1.1 Film

Let us start by considering the spectroscopy of a thin film, without the deposition of a gold metasurface. The average transmission amplitude is shown in Figure 1.1. The corresponding real conductivity is estimated from the transmission magnitude  $|t|$ ,

$$\sigma = \frac{1 + n_s}{Z_0 d} \frac{1 - |t|}{|t|}$$

with film thickness  $d = 10.8$  nm, and refractive index  $n_s = 4.8$  of the substrate. The conductivity is shown on the secondary axis in Figure 1.1.

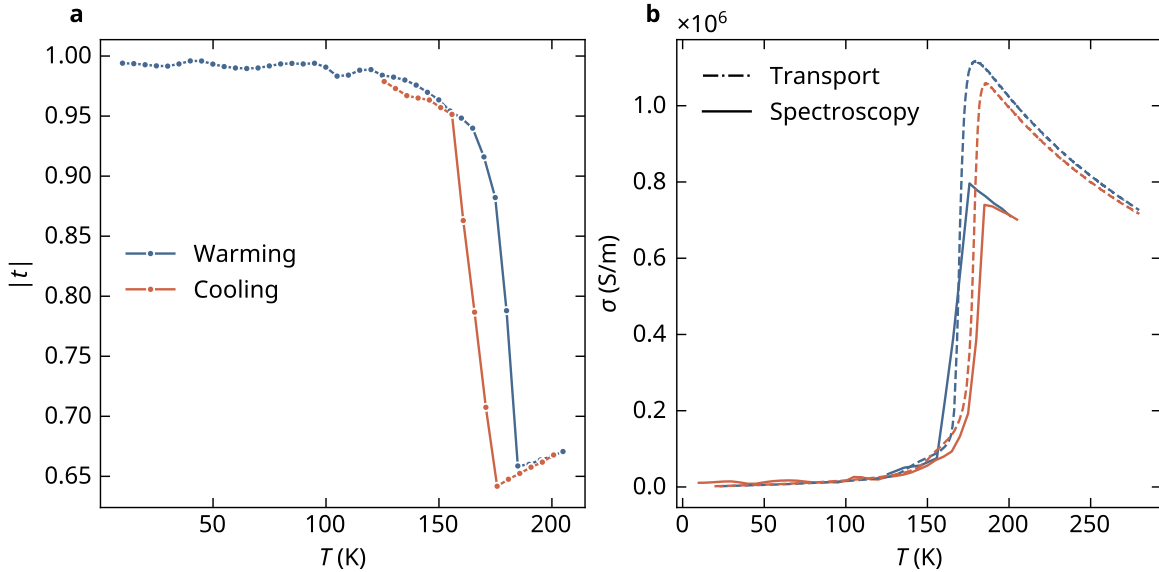


Figure 1.1: The temperature dependence of the average transmission amplitude of the film, for both heating directions.

## 1.2 Metasurface

After depositing a gold metasurface on the film, the transmission amplitude is shown in Figure 1.2. This amplitude is defined as the ratio of the spectrum of a waveform transmitted through the sample  $\hat{S}_{\text{sam}}(T)$  to the spectrum of a waveform transmitted through a reference substrate  $\hat{S}_{\text{sub}}(T)$ ,

$$\hat{t} = \frac{\hat{S}_{\text{sam}}(T)}{\hat{S}_{\text{sub}}(T)} \quad (1.1)$$

In panel **b** of Figure Figure 1.2 is shown the amplitude at 1 THz as a function of temperature for the two temperature sweep directions. Notice that no hysteresis is present.

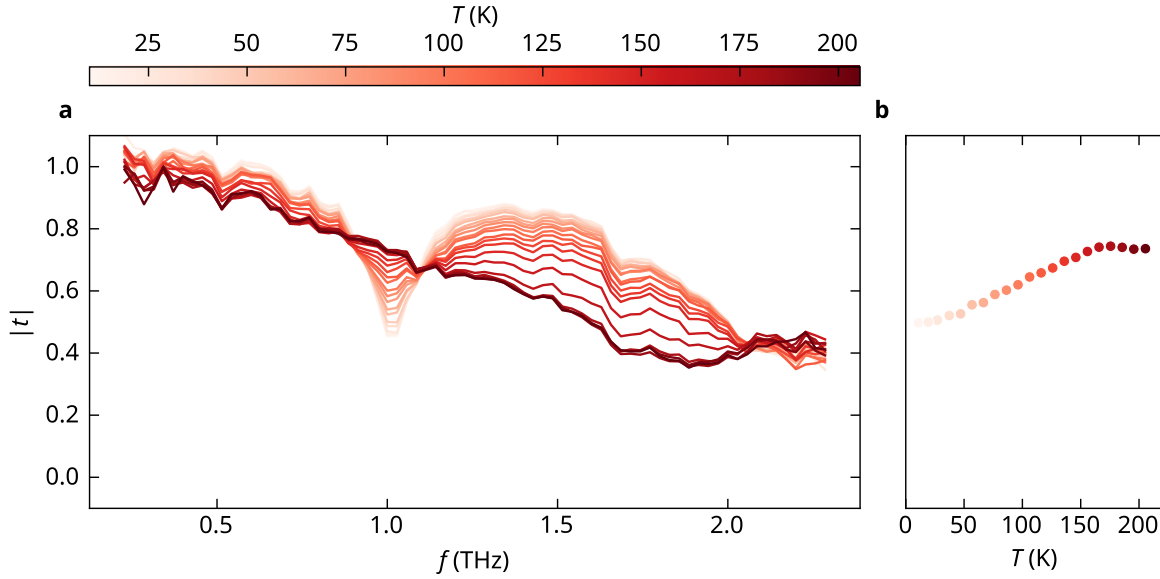


Figure 1.2: The transmission amplitude spectra for a set of temperatures, for both heating directions (cooling, -1, and heating, +1).

We know from transport measurements that the sample exhibits a clear metal-to-insulator transition around 170 K. This transition temperature is not easily identifiable from Figure 1.2 **b**, but will become clear when we convert the transmission amplitude to conductivity.

## 1.3 Calculations

The transmission amplitude of the sample was calculated theoretically, assuming a homogeneous conductivity across the sample. A subset of the calculated transmission amplitude

spectra is shown in Figure 1.3.

cond_gap f64	cond_film f64	freq f64	t.real f64	t.imag f64
100.0	146.0	0.2	0.9939092	-0.062831
100.0	146.0	0.256	0.991093	-0.081497
100.0	146.0	0.311	0.987555	-0.100842
100.0	146.0	0.366	0.983047	-0.120582
100.0	146.0	0.42	0.977913	-0.140637
...	...	...	...	...
912000.0	1e6	2.063	0.385546	0.0882
912000.0	1e6	2.095	0.38966	0.085757
912000.0	1e6	2.129	0.393373	0.084034
912000.0	1e6	2.165	0.3971802	0.082684
912000.0	1e6	2.203	0.4008718	0.081284

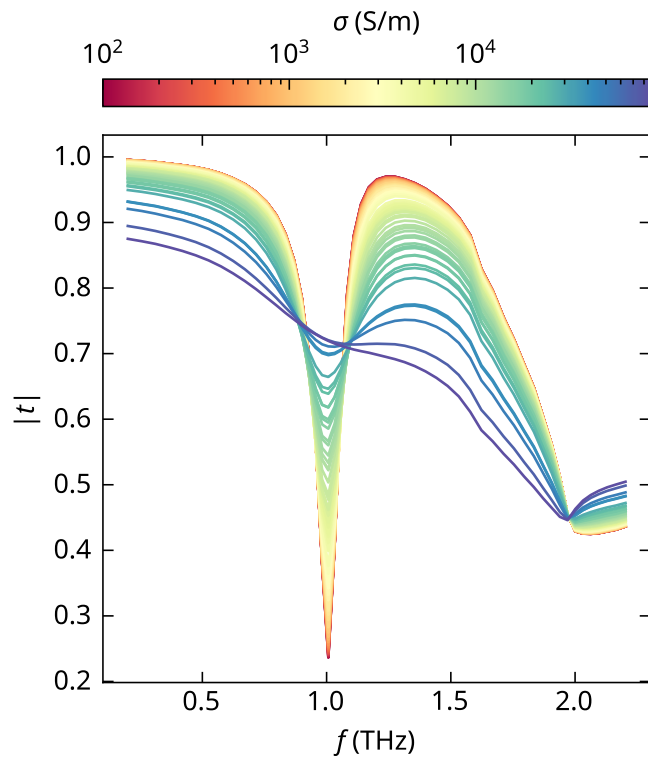


Figure 1.3: A subset of the calculated transmission amplitude spectra, for a set of conductivities.

We want to extract the conductivity  $\sigma$  from the calculations, at each experimental temperature  $T$ . To enhance the match between calculation and experiment, it is helpful to consider the *relative transmission amplitude* rather than the absolute:

$$\hat{t}_r(T) \equiv \frac{\Delta\hat{t}}{\hat{t}_0} = \frac{\hat{S}(T) - \hat{S}_0}{\hat{S}_0} \quad (1.2)$$

This removes any hidden response functions from the experiment that were not successfully deconvolved from the signal. We choose  $\hat{S}_0 = \hat{S}(T_{\min})$  with  $T_{\min}$  being the base temperature of the optical cryostat of about 10 kelvin.

Similarly, for the calculation, the relative transmission amplitude is

$$\hat{t}_r(\sigma, \sigma_0) \equiv \frac{\Delta\hat{t}}{\hat{t}_0} = \frac{\hat{S}(\sigma) - \hat{S}(\sigma_0)}{\hat{S}(\sigma_0)} \quad (1.3)$$

where  $\sigma_0$  is the conductivity of the sample at the base temperature  $T_{\min}$ , which is not known *a priori*. By moving to this relative representation, we add one extra unknown to our problem, namely the value of  $\sigma_0 = \sigma(|t|)$ , which is a shared parameter for all temperatures  $T$ .

We seek to find  $\sigma_0$  and  $\{\sigma\}_T$  that solves

$$\min_{\sigma_0} \frac{1}{N} \sum_{i=1}^N \min_{\sigma} \|\hat{t}_{r,\text{meas}}(T_i) - \hat{t}_{r,\text{calc}}(\sigma, \sigma_0)\| \quad (1.4)$$

where  $\|\cdot\|$  is the norm over the frequency domain. The calculations of the relative transmission amplitude are performed on a dense grid of  $\sigma$ , and cubic interpolation is used to estimate the relative transmission amplitude at arbitrary conductivities.

To find the optimal reference conductivity ( $\sigma_0$ ), we perform the inner minimization for each candidate  $\sigma_0$  to obtain the optimal set  $\{\sigma\}_T$ , in the sense of minimizing the residual sum of squares. This gives us an outer error measure  $\varepsilon_{\sigma_0}$  for each candidate  $\sigma_0$ ,

$$\varepsilon(\sigma_0) = \frac{1}{N} \sum_{i=1}^N \min_{\sigma} \|\hat{t}_{r,\text{meas}}(T_i) - \hat{t}_{r,\text{calc}}(\sigma, \sigma_0)\| \quad (1.5)$$

which we plot in Figure 1.5.

Fortunately this has a global minimum, and we have a good estimate for the reference conductivity  $\sigma_0$ . Fixing this  $\sigma_0$ , we can go back and explore the error landscape in the space of  $\sigma$ ,

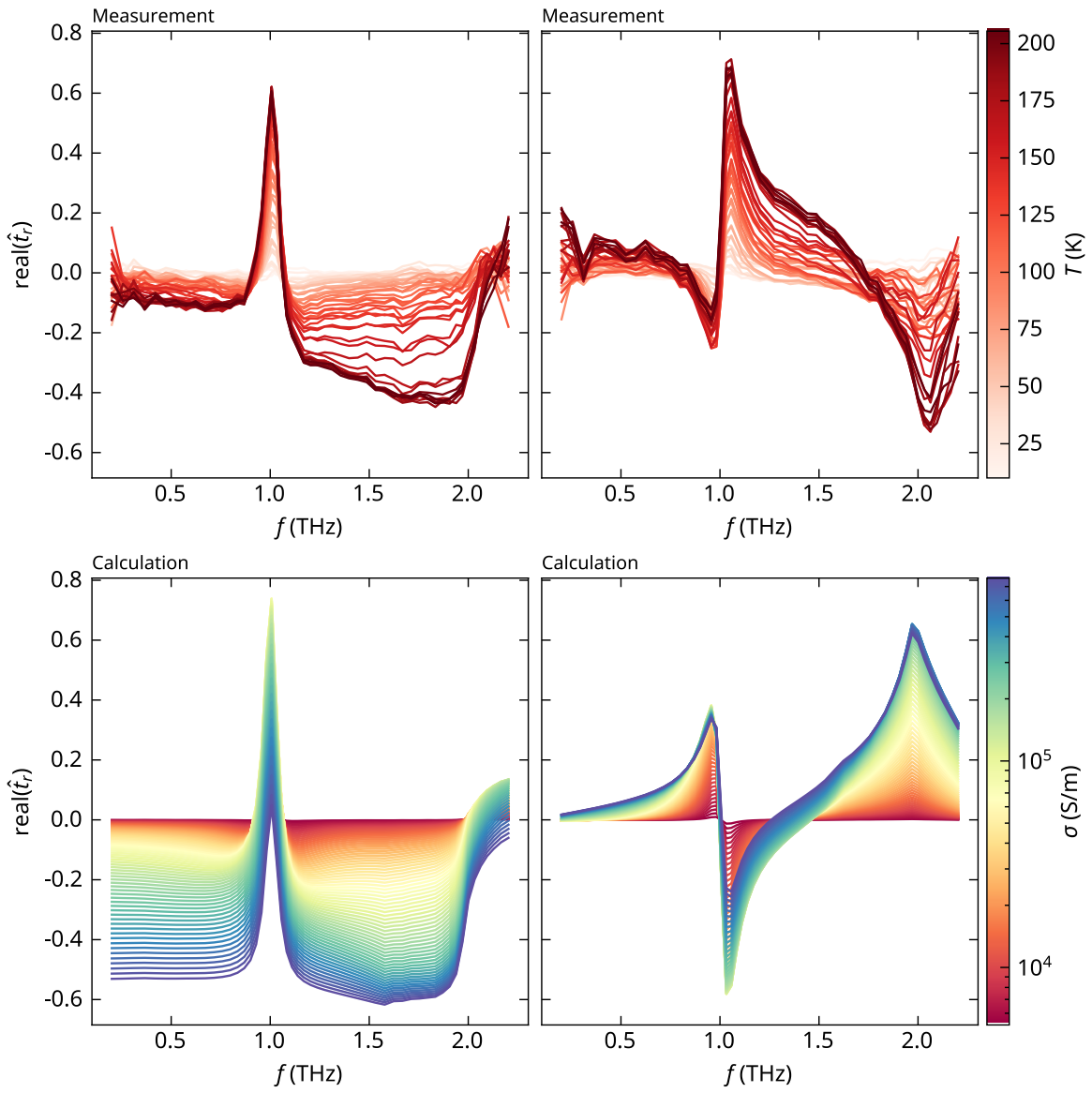


Figure 1.4: To the left, the experimental relative spectra; to the right, the calculated relative spectra, for a fixed choice of  $\sigma_0$ .

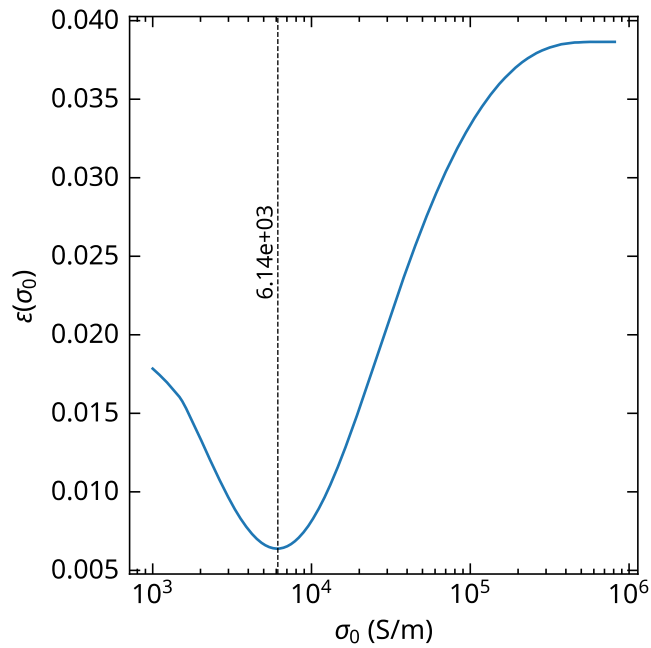


Figure 1.5: The aggregate error as defined in Equation 1.5, as a function of the reference conductivity  $\sigma_0$ .

$$\varepsilon(\sigma, T) = \|\hat{t}_{r,\text{meas}}(T) - \hat{t}_{r,\text{calc}}(\sigma)\|_2 \quad (1.6)$$

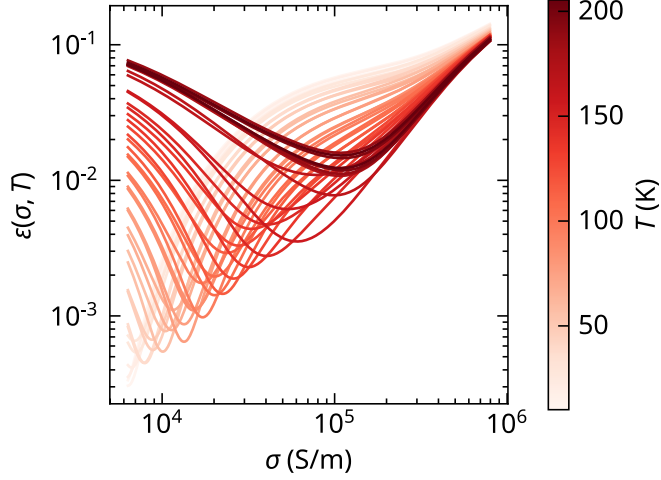


Figure 1.6: The aggregate error as defined in Equation 1.5, as a function of the reference conductivity  $\sigma$ .

The error is larger at higher temperatures, since that is where the relative transmission amplitude is also the largest. But there is at least one minimum for each temperature, and we get good estimates for the conductivity at each temperature. There is a local minimum around  $\sigma = 3 \times 10^3$  which is temperature independent, and therefore not physical. We therefore restrict the minima to  $\sigma > 3 \times 10^3$ , and obtain unique solutions.

We inspect the  $\hat{t}_r$  experimental and calculated distributions, and the corresponding residuals, in Figure 1.4.

The residuals are small, and the match between calculation and experiment is acceptable, aside from a systematic error related to an overall slope. The final mapping from temperature to conductivity is shown in Figure 4.3.

## 1.4 Metasurface with finite scattering time

The above analysis uses a constant, and real, conductivity  $\sigma$  for the film. In reality, the conductivity is frequency dependent,

$$\sigma(\omega) = \frac{\sigma_{\text{dc}}}{1 - i\omega\tau}$$

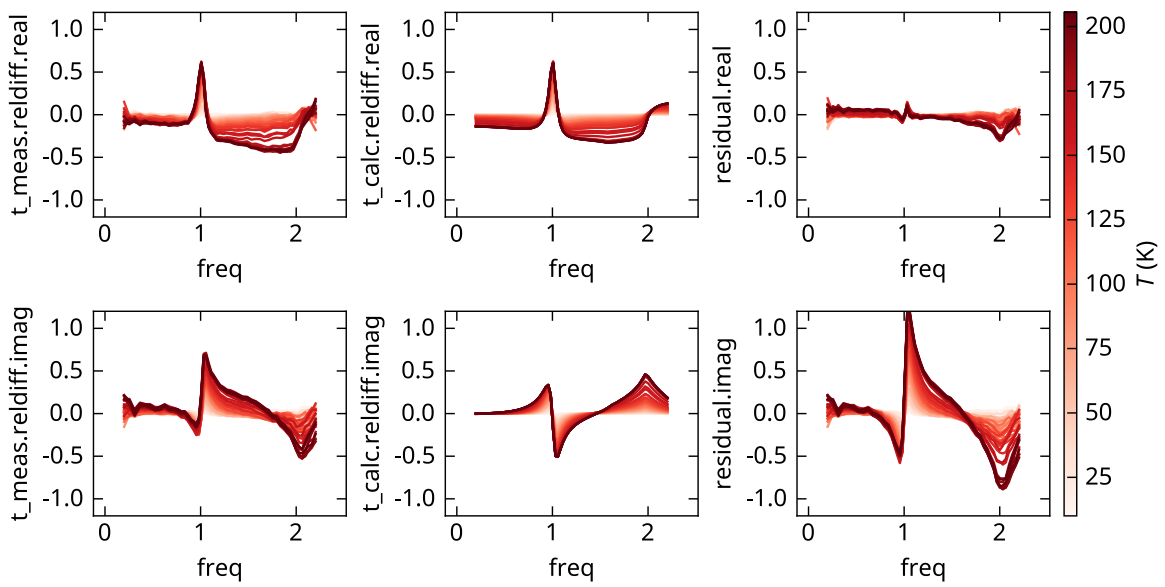


Figure 1.7: Solution to Equation 1.4. To the left, the experimental relative spectra; in the middle the calculated relative spectra, and to the right the residuals.

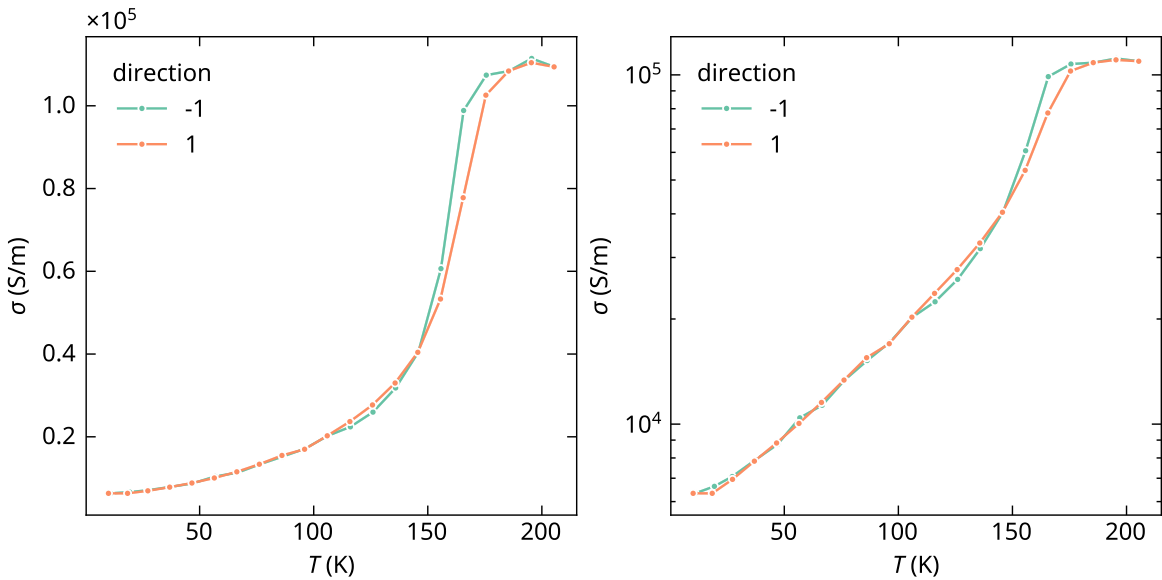


Figure 1.8: The mapping that solves Equation 1.4.

where  $\sigma_{dc}$  is the DC conductivity, and  $\tau$  is an electronic scattering time. Again, using the relative transmission amplitude requires us to find the reference values  $\sigma_0$  and  $\tau_0$  that minimizes the outer error as defined in Equation 1.5. A colormap of this error is shown in Figure 1.9.

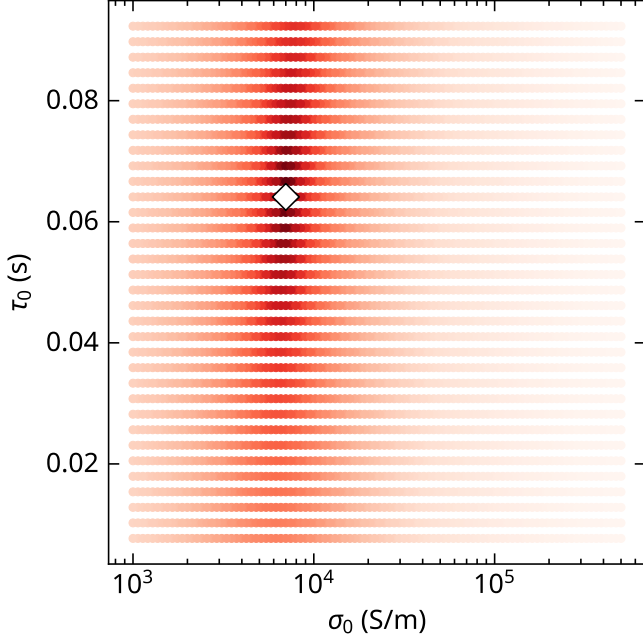


Figure 1.9: Color map of the logarithm of the aggregate error as defined in Equation 1.5, as a function of the reference conductivity  $\sigma_0$  and scattering time  $\tau_0$ . A clear minimum is present at  $\tau_0 \approx 60$  fs and  $\sigma_0 = 7e4$  S/m. This is used as the reference parameters for the subsequent analysis, and the scattering time  $\tau_0$  is assumed equal at all temperatures.

Having identified a minimum for the reference parameters, we proceed to fix  $\tau = \tau_0$  across all temperatures, and select the minimizing values for  $\sigma$  at each temperature. The resulting mapping is shown in Figure 1.10.

Overall, we find that including this finite scattering time slightly improves the match between calculation and experiment (i.e. a slightly smaller residual), particularly in the imaginary part of the transmission amplitude.

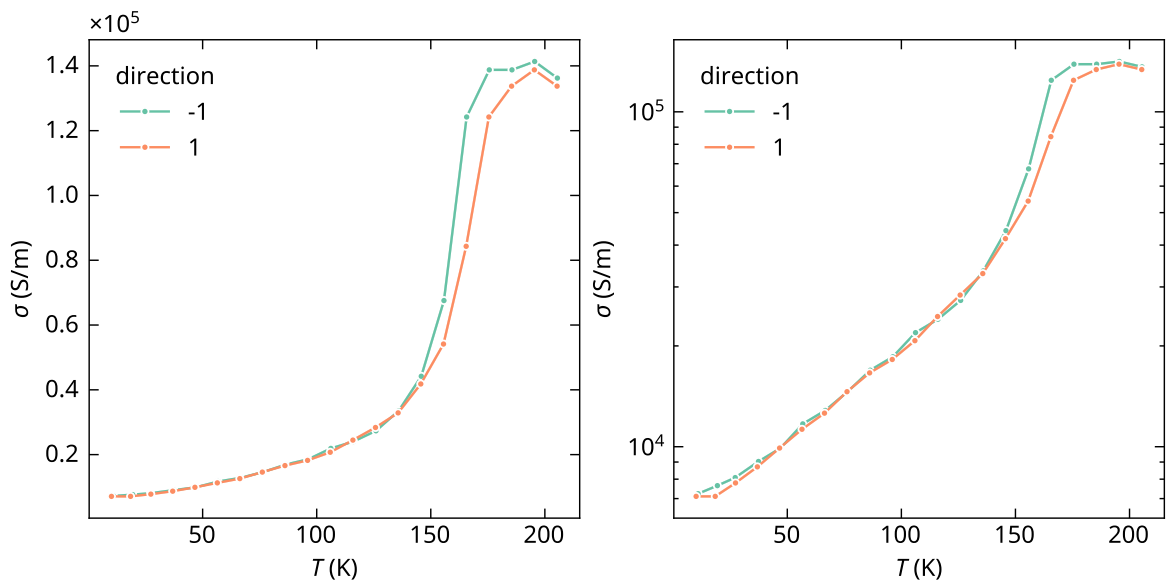


Figure 1.10: The mapping that solves Equation 1.4.

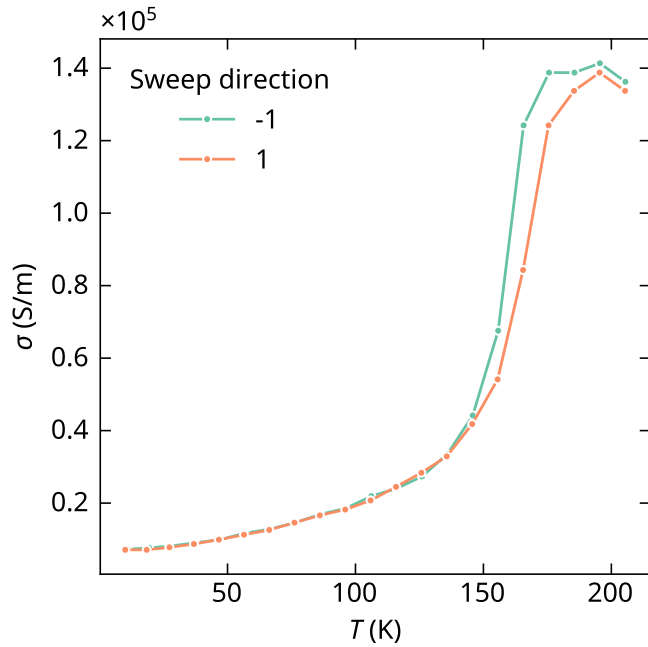


Figure 1.11: The mapping that solves Equation 1.4.

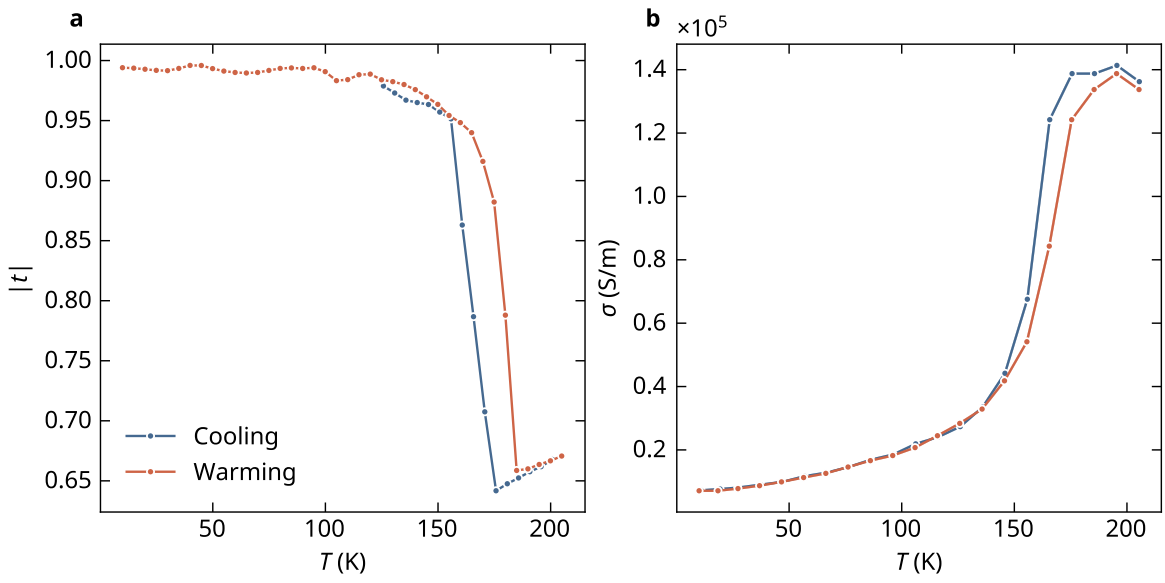


Figure 1.12: The temperature dependence of the average transmission amplitude of the film, for both heating directions.

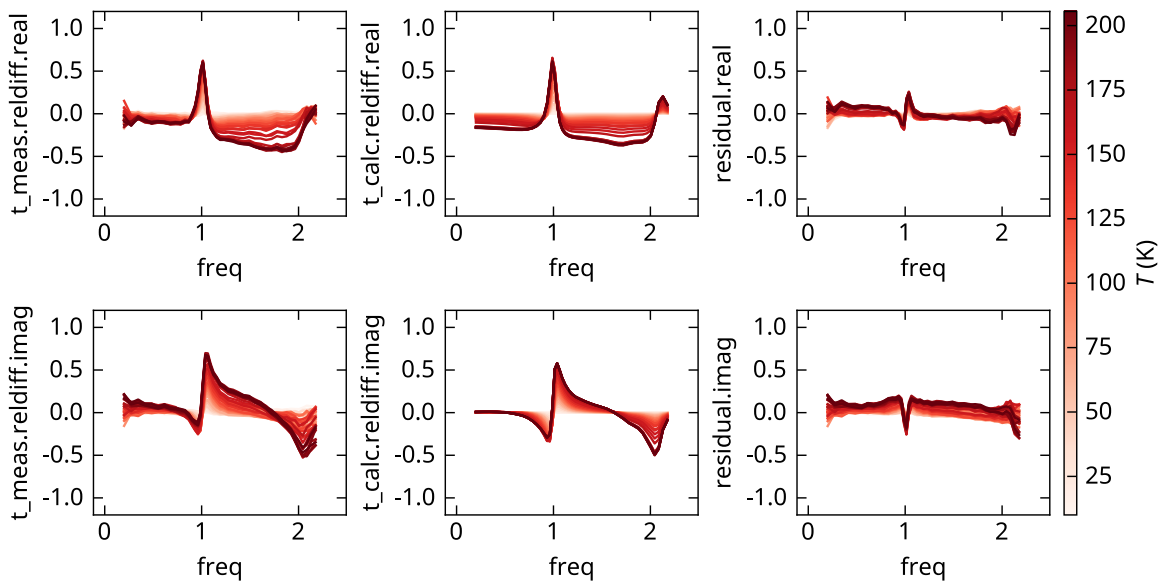


Figure 1.13: Comparison of film (left) and metasurface (right).

## 2 Sample comparisons

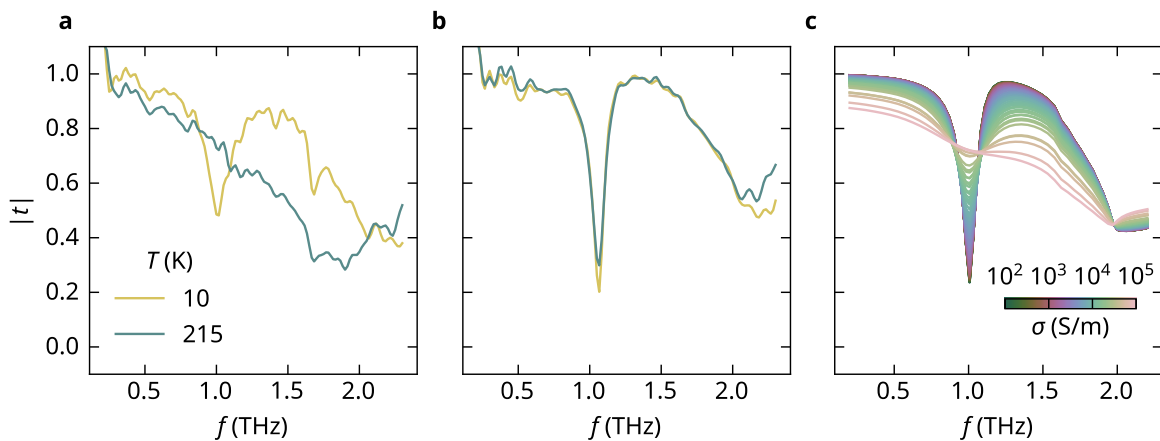


Figure 2.1: Comparison of the transmission spectra of **a.** Resonators on thin film. **b.** Resonators on a bare substrate. Transmission through a blanket substrate is used as reference.

### 3 Substrate

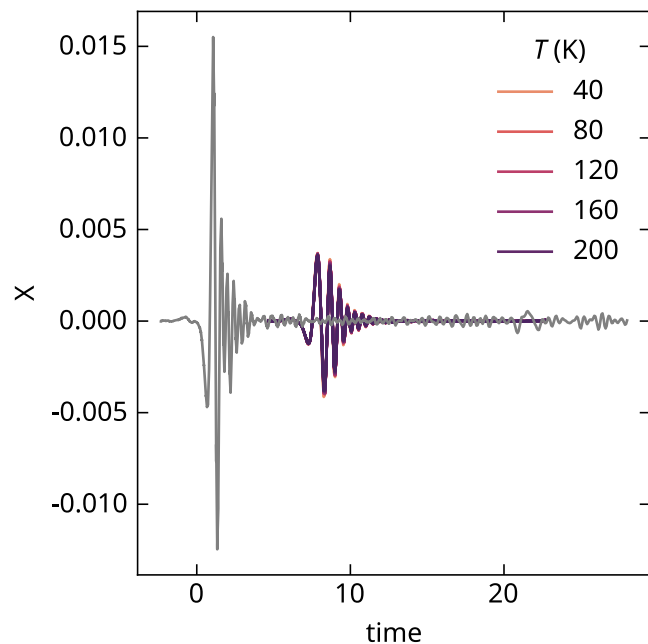


Figure 3.1: Time-domain signals of the LSAT substrate and the no-sample reference (gray).

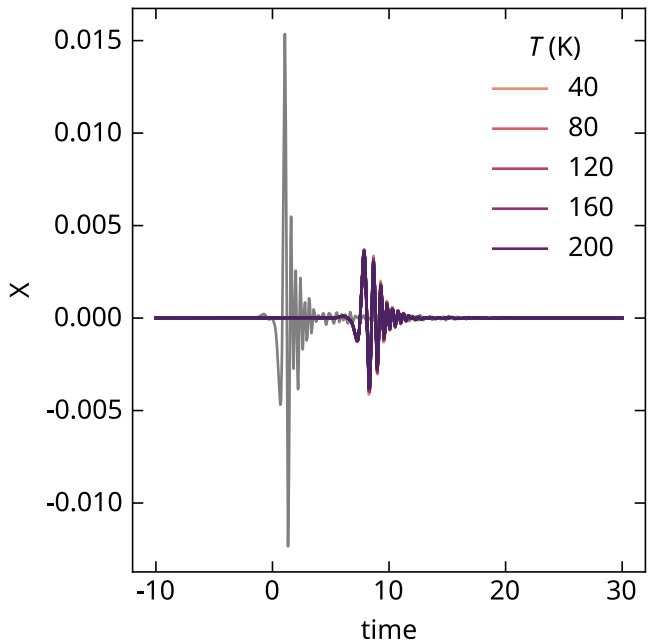


Figure 3.2: Interpolated waveforms of the LSAT substrate and the no-sample reference (gray), with windowing.

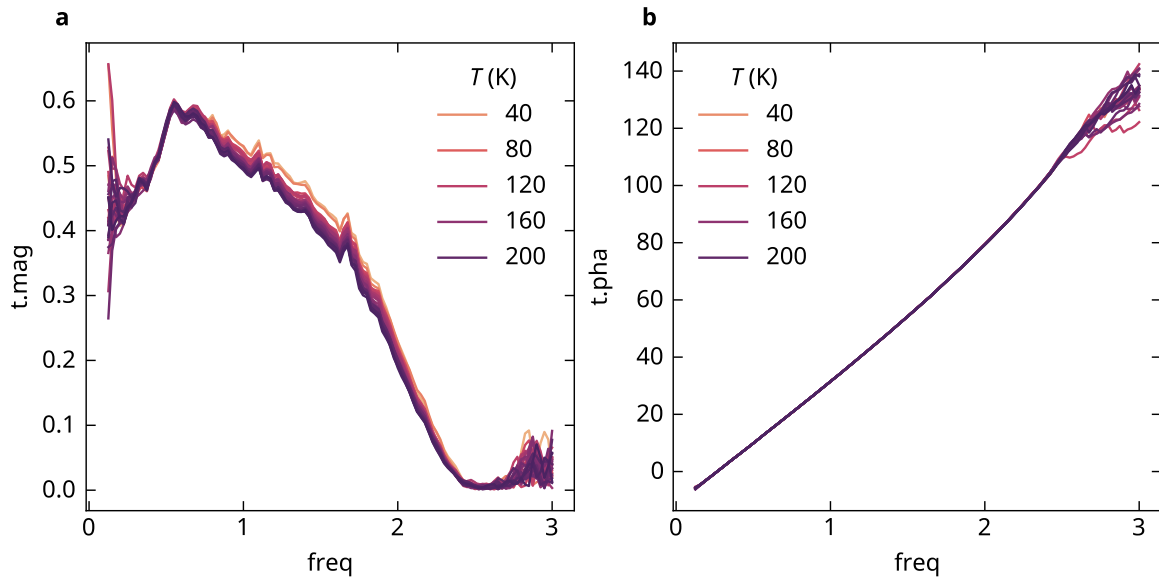


Figure 3.3: Substrate spectra, defined as the ratio of the Fourier transforms of the waveforms transmitted through the substrate, to that of the no-sample reference. **a.** Magnitude. **b.** Phase.

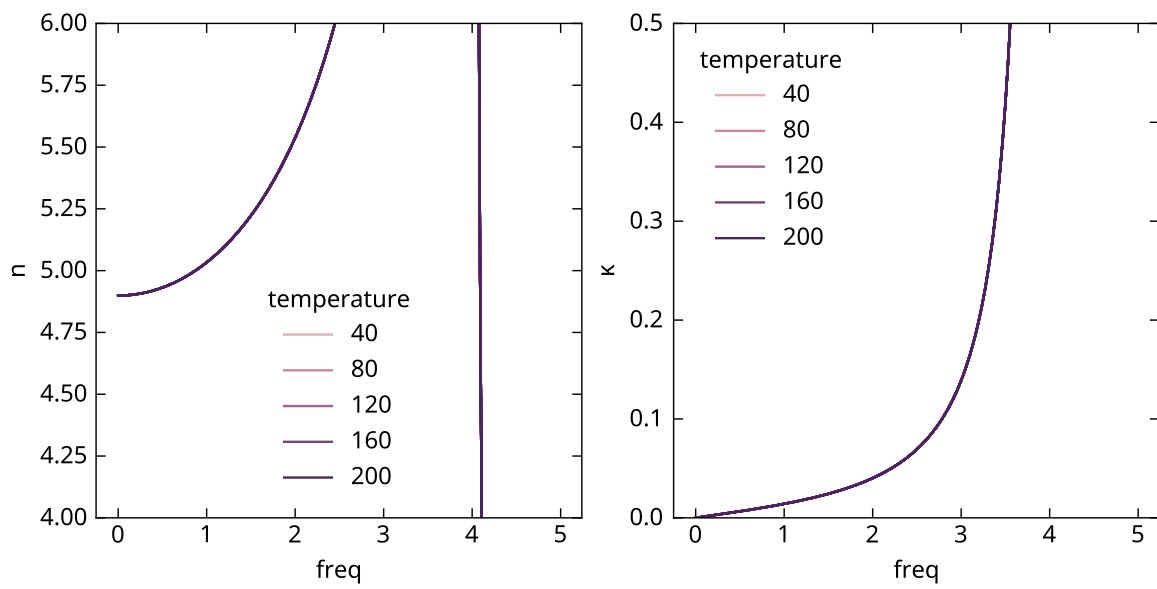


Figure 3.4: Fit of the substrate spectra to a Drude-Lorentz model, using a single resonance. **a.** Real part of the refractive index. **b.** Imaginary part of the refractive index.

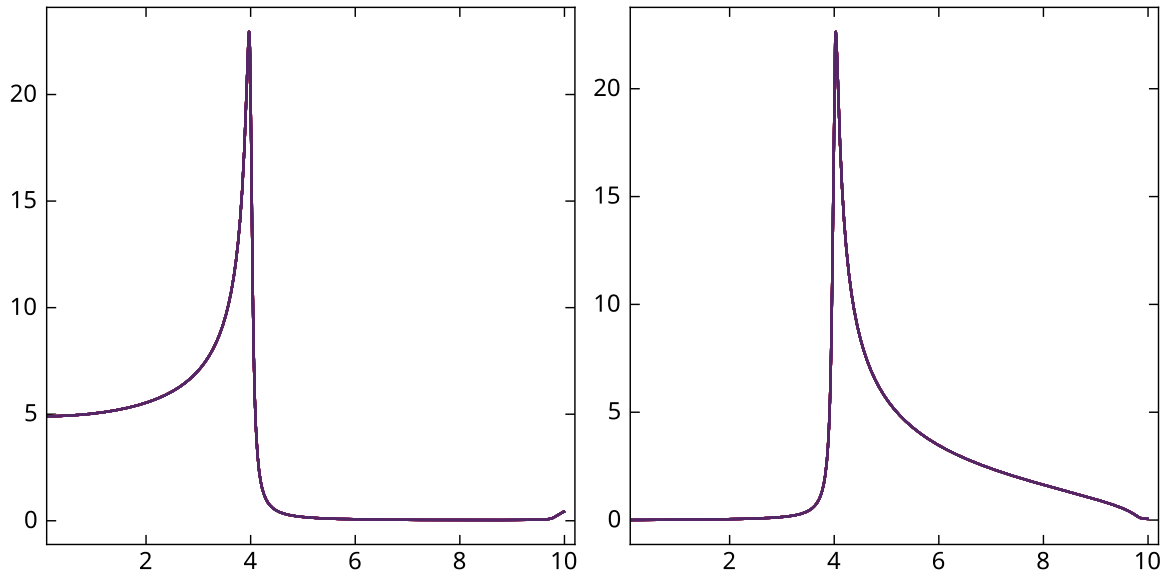


Figure 3.5: A wide view of the fit result.

## **Part II**

# **Dynamics**

# 4 Pump-probe overlap

## 4.1 Experiment

Waveforms transmitted through the sample is recorded for a set of pump-probe delays  $\tau$  (the common delay line of the optical gate and THz probe, with respect to the THz pump), sampled densely around  $\tau = 0$ . The pump is modulated, so that the signal is the differential signal (pump on minus pump off). A reference waveform without pump is measured as well, so that we have both  $\Delta E$  and  $E$ .

We load the raw data from experiment, and pad with zeros to interpolate in the frequency domain. Note that these measurements were quite noisy, since a lot of time-traces had to be performed for combinations of the waveplate position (pump power) and pump-probe delay. The dataset is structured as follows:

pp_delay	time	dX	X
f64	f64	f64	f64
1.6008	-10.0	0.0	-0.0
1.6008	-9.997	0.0	-0.0
1.6008	-9.994	0.0	-0.0
1.6008	-9.991	0.0	-0.0
1.6008	-9.988	0.0	-0.0
...	...	...	...
-0.8004	49.985	0.0	-0.0
-0.8004	49.988	0.0	-0.0
-0.8004	49.991	0.0	-0.0
-0.8004	49.994	0.0	-0.0
-0.8004	49.997	0.0	-0.0

The time-domain data is transformed to the frequency domain. The measured signal is the differential signal (pump on minus pump off), and one trace of the absolute waveform absent pump. We therefore look at the relative transmission amplitude in the frequency domain, defined as

$$\hat{t}_r(\tau) \equiv \frac{\Delta \hat{t}}{\hat{t}_0} = \frac{\Delta \hat{S}(\tau)}{\hat{S}_0} \quad (4.1)$$

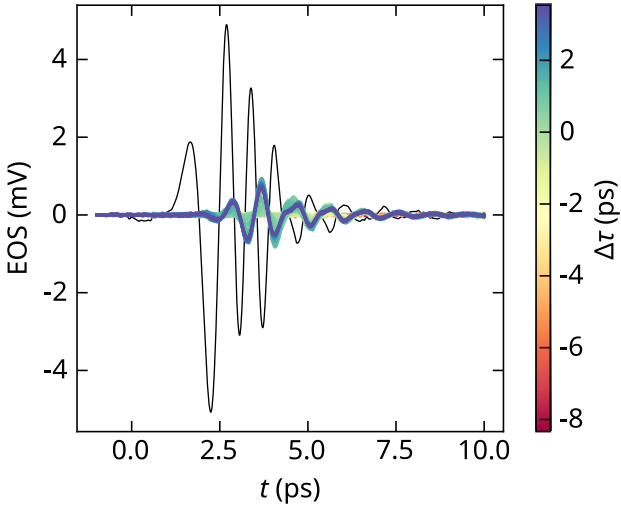


Figure 4.1: Summary of raw waveforms, recorded after transmission through the sample for various values of the THz pump field strength, and the pump-probe delay.

Here,  $\hat{S}$  is the discrete Fourier transform of a waveform,  $\tau$  is the pump-probe delay, and  $\mathcal{E}$  the pump field strength. The dependence on frequency is omitted in the notation.  $\Delta\hat{S}$  is the Fourier transform of the differential waveform, and  $\hat{S}_0$  is the transform of the full waveform absent pump.

## 4.2 Calculations

The transmission amplitude of the sample can be calculated theoretically, with the simplifying assumption that any field-induced variation in conductivity occurs exclusively in the capacitor-like gap of the split-ring resonator.

The calculated data is aligned with the measured data, on the frequency axis (same frequency sampling), and upsampled along the conductivity axis through spline interpolation.

Then, it is relativized with respect to the low-temperature conductivity of the film (and resonator gap), as determined from the linear spectroscopy temperature study of the sample. This coincides with the negative-delay spectrum of the experiment, so that the reference spectra are the same for both measured and calculated data.

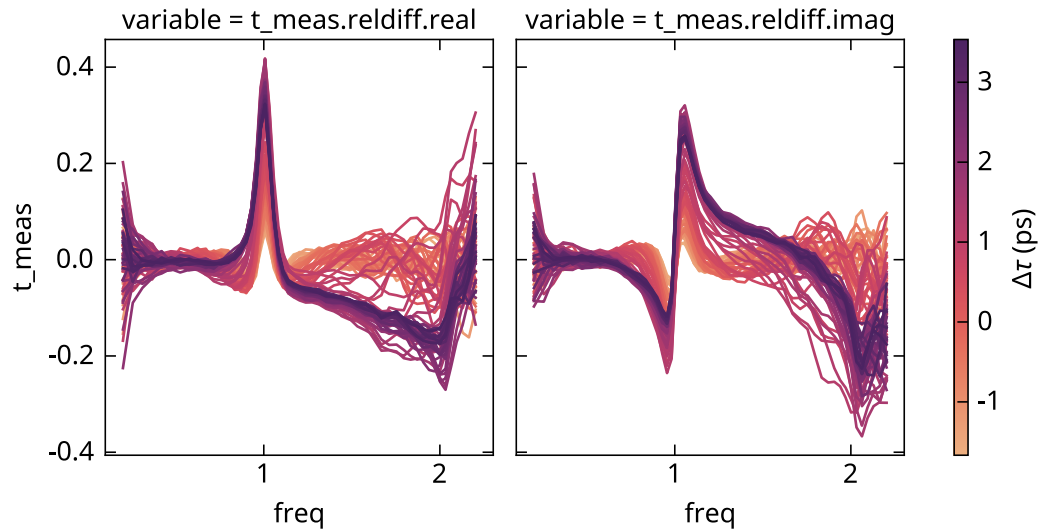
pp_delay f64	cond_gap f64	freq f64	t_meas.reldiff.real f64	t_meas.reldiff.imag f64	t_calc.reldiff.real f64	t_calc.reldiff.imag f64
-8.3375	3182.395249	0.2	-0.052035	0.010738	-0.000041	0.000036
-8.3375	3182.395249	0.256	-0.056813	-0.03299	0.000187	-0.000104

pp_delay	cond_gap	freq	t_meas.reldiff.real	t_meas.reldiff.imag	t_calc.reldiff.real	t_calc.reldiff.imag
f64	f64	f64	f64	f64	f64	f64
-8.3375	3182.395249	0.311	0.009847	-0.028353	0.000099	0.000012
-8.3375	3182.395249	0.366	0.000878	0.013035	-0.000035	-0.000017
-8.3375	3182.395249	0.42	-0.006976	-0.002282	-0.000016	0.000005
...	...	...	...	...	...	...
3.5351	745321.206338	2.063	-0.080798	-0.226333	-0.100646	-0.566836
3.5351	745321.206338	2.095	-0.078631	-0.183315	-0.033345	-0.52609
3.5351	745321.206338	2.129	-0.085724	-0.14683	0.020898	-0.483274
3.5351	745321.206338	2.165	-0.036317	-0.157965	0.068303	-0.440767
3.5351	745321.206338	2.203	0.074201	-0.176202	0.107259	-0.393834

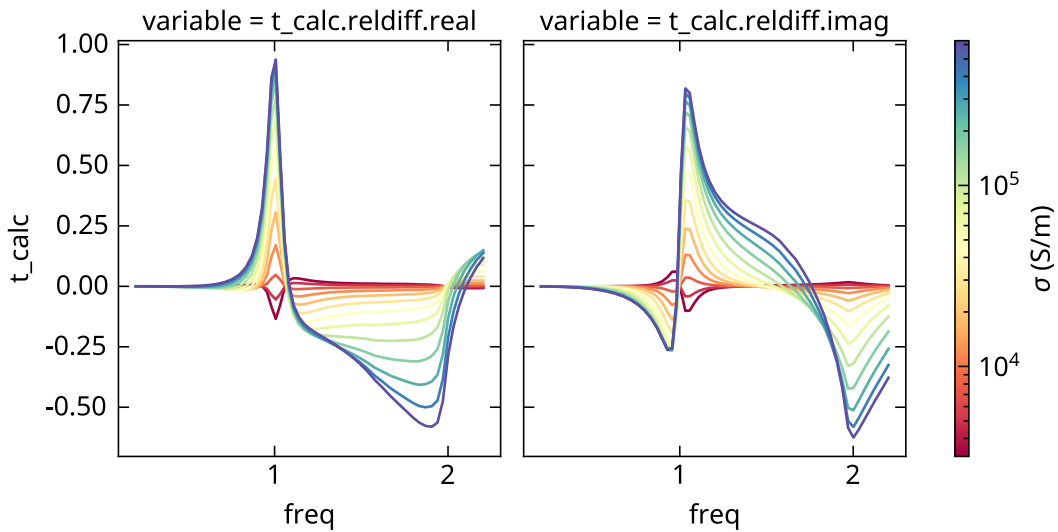
### 4.3 Mapping

Finally, we can map from the experimental parameter ( $\tau$ ) to the computational one ( $\sigma$ ). The minimization norm is a residual sum of squares (RSS), but the minimization is done in a single step “grid search”, rather than iteratively. This is possible because the calculations are done on a conductivity grid a priori, and interpolation is reliable. The minimization is done as follows:

1. The residual sum of squares (RSS) is calculated by grouping by  $\tau$  and  $\sigma$ , squaring and summing the residual over frequencies.
2. Grouping by  $\tau$  only, the RSS is sorted in ascending order (together with  $\sigma$ ) and the smallest value is picked.



(a) Experimental data, with transmission relative to an unexcited sample at base temperature.



(b) Calculated data, with transmission relative to a sample with homogeneous conductivity, corresponding to base temperature.

Figure 4.2: Relative transmission amplitude

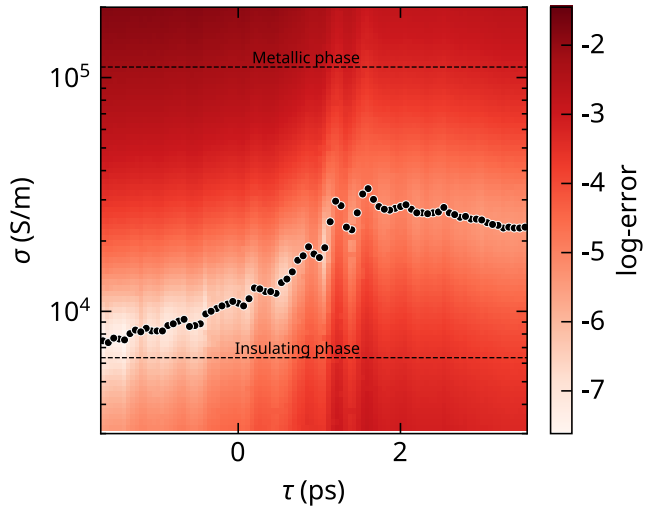
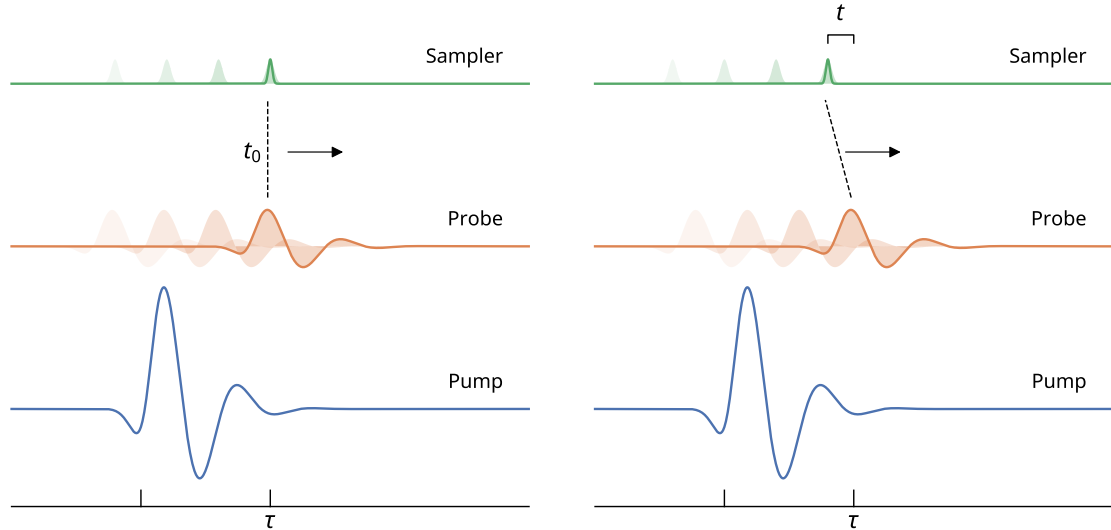


Figure 4.3: In black, the least-residual  $\sigma$ , and in color the residual sum of squares (RSS).

#### 4.4 Scan type illustrations



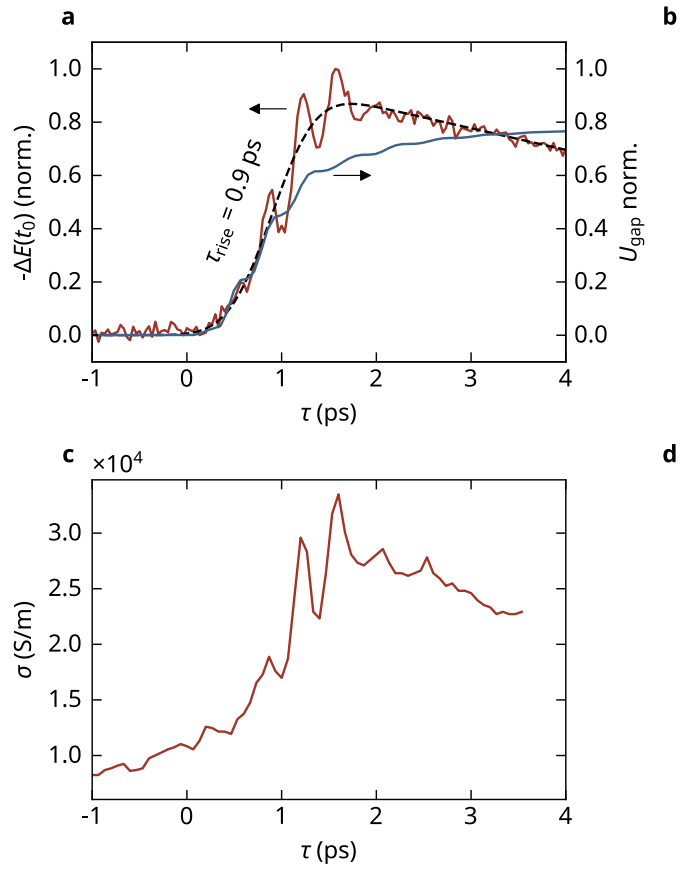
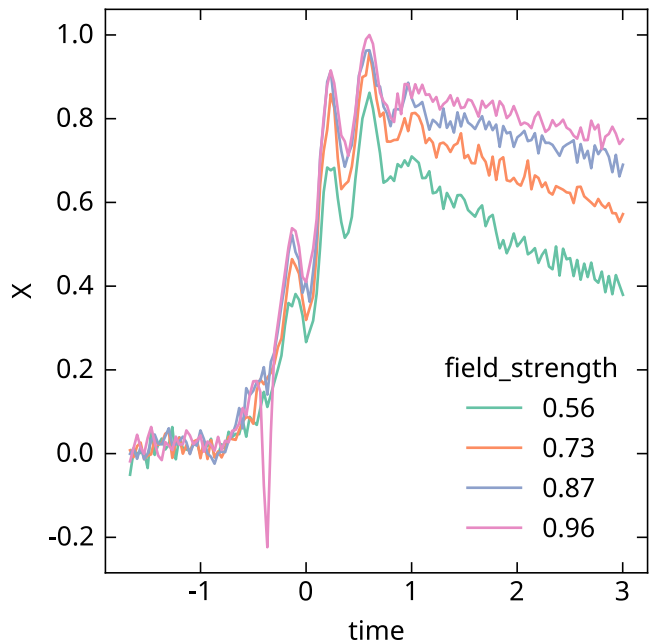


Figure 4.4: A 1D-scan, probing a singular point in time on the probe waveform, as a function of the delay time  $\tau$  between the THz pump and THz probe pulses.

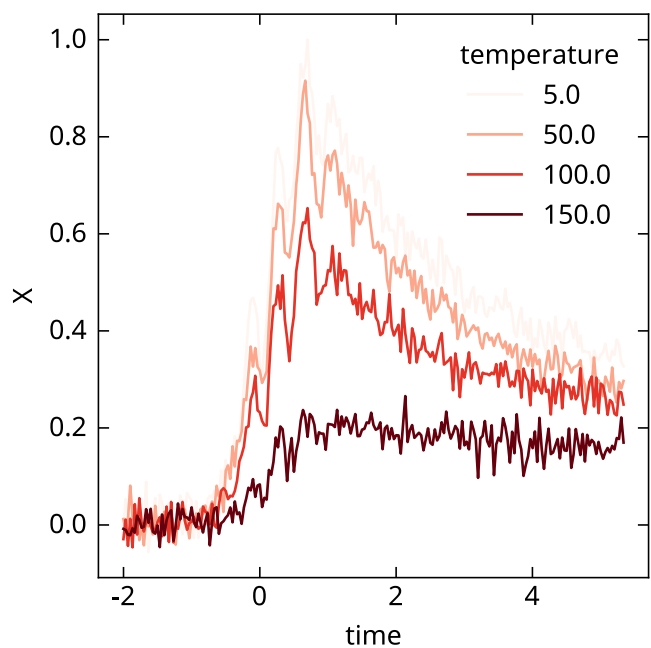
## 4.5 1D scan

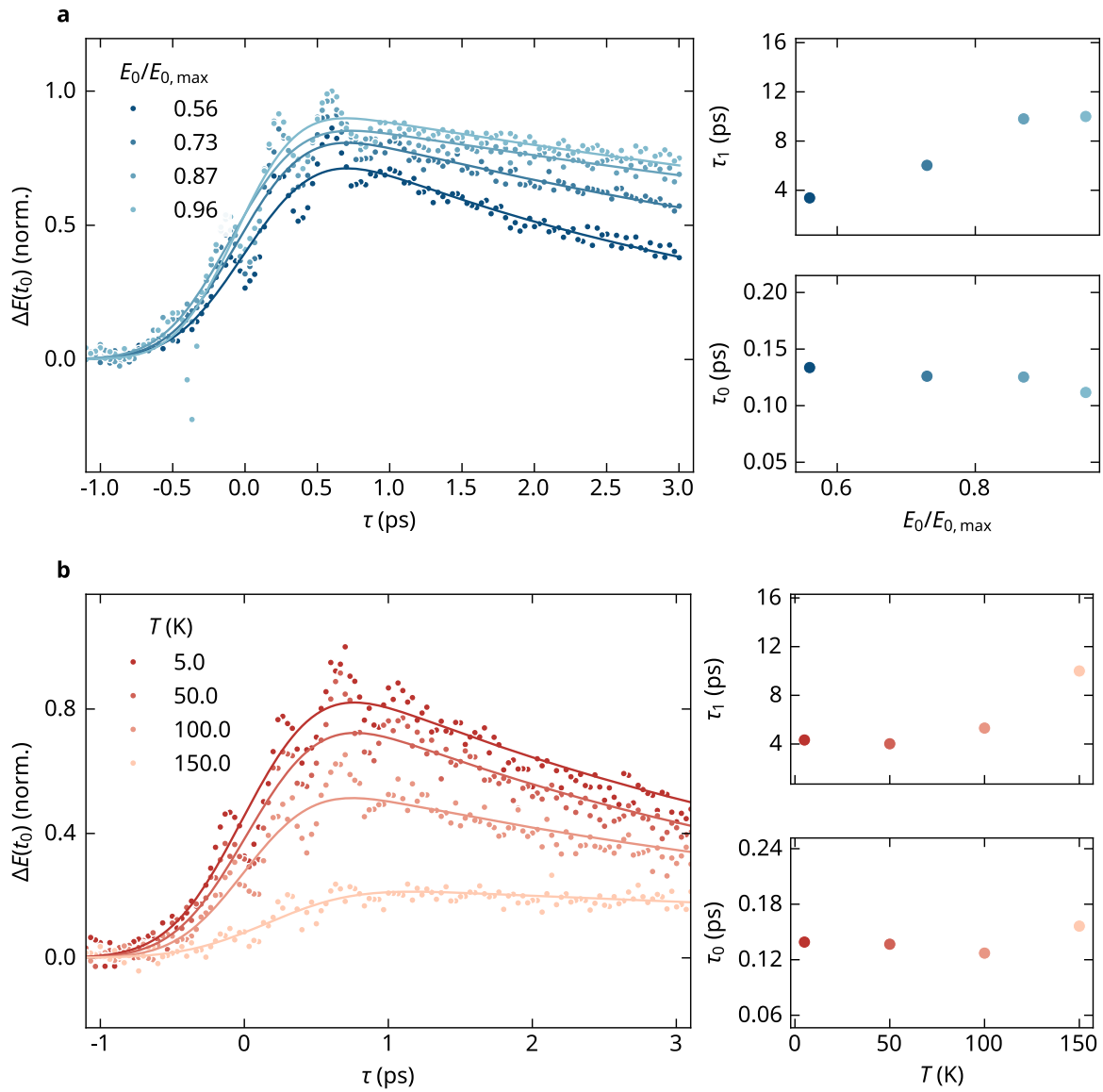
## 4.6 Rise and decay time scaling

### 4.6.1 Field strength dependence



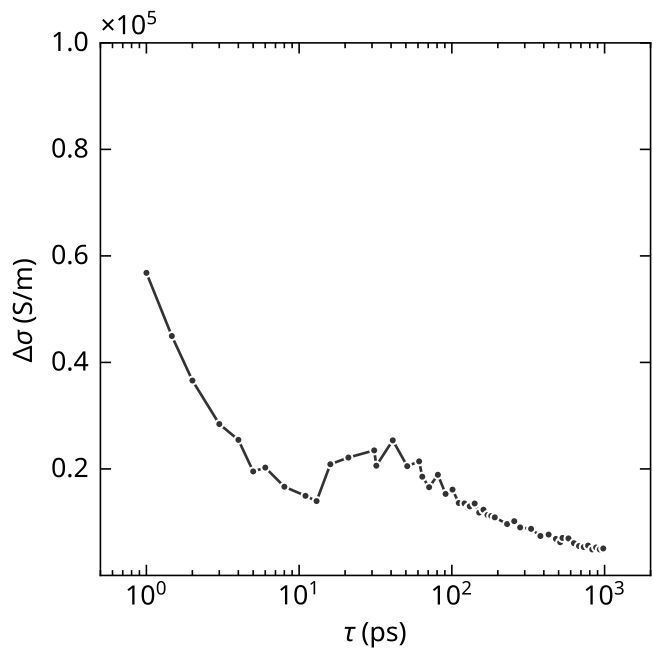
#### 4.6.2 Temperature dependence





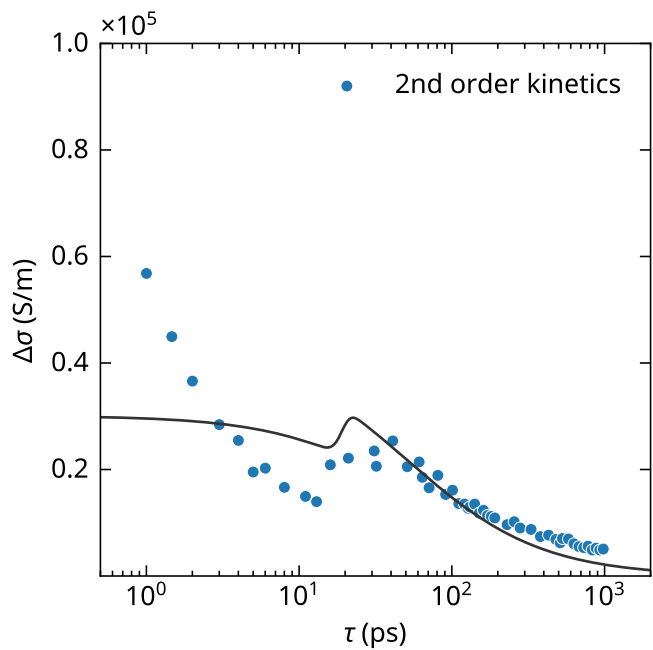
## 5 Decay dynamics

### 5.1 2D scans



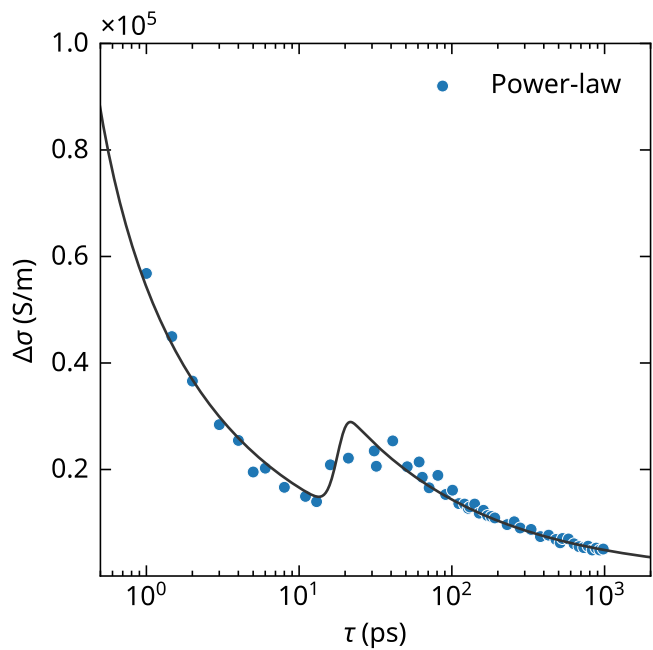
#### 5.1.1 Second-order kinetics

$$\frac{d\sigma}{dt} = -k\sigma^2$$

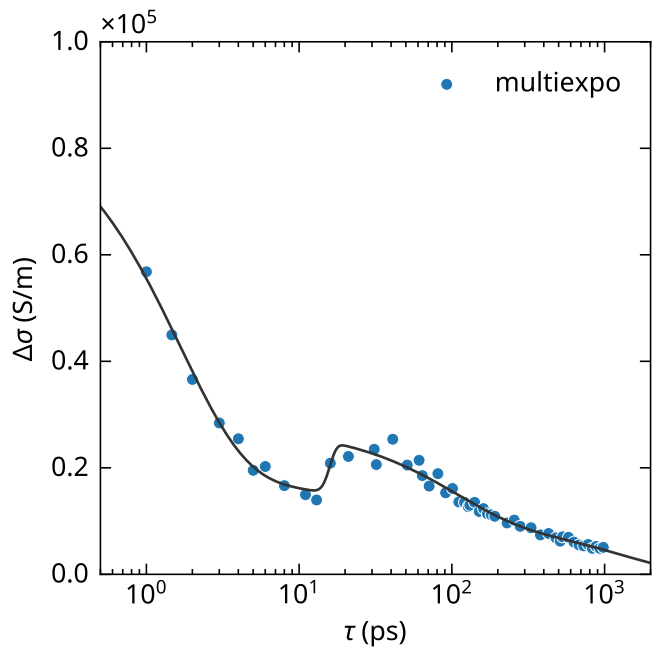


### 5.1.2 Power-law decay

$$\sigma(t) = \frac{\sigma_0}{(t/\tau_0)^\alpha}$$



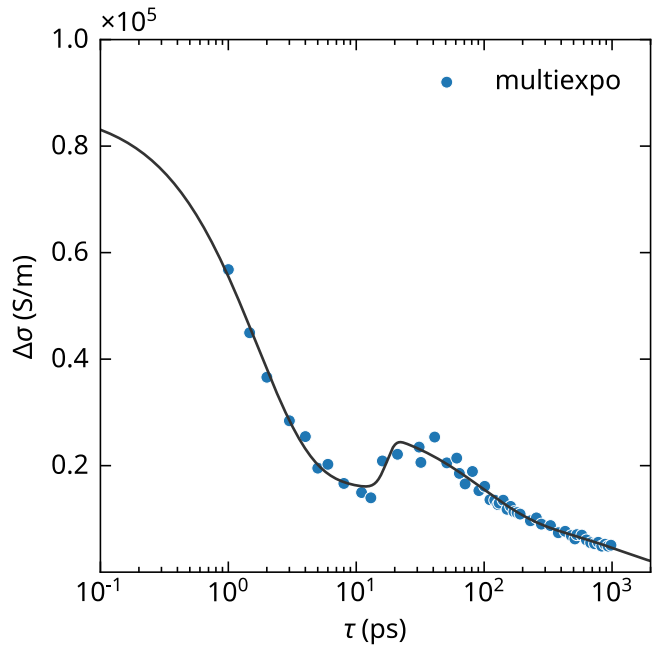
### 5.1.3 Multi-exponential decay, segregated



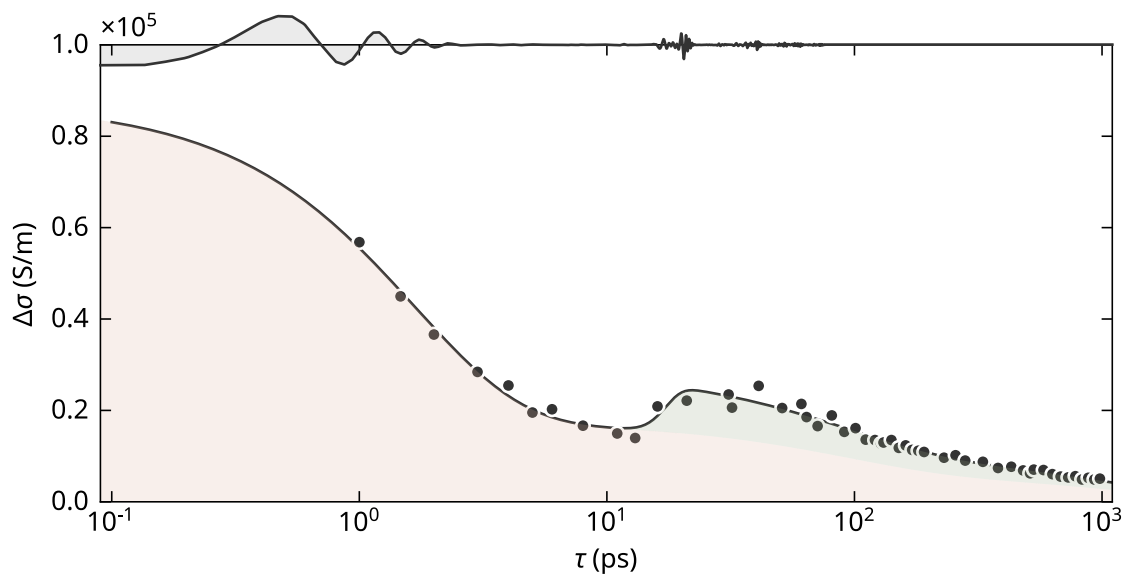
### 5.1.4 Multi-exponential decay

Table 5.1: Parameters

name	value	initial value	min	max	vary
t_pump	0.00927652	0	-1.00000000	1.00000000	True
amp1	69431.7968	70000.0	1000.00000	1000000.00	True
amp2	11133.7118	20000.0	1000.00000	1000000.00	True
amp3	6018.48164	10000.0	0.00000000	10000.0000	True
tau1	1.66754065	3	0.10000000	10.0000000	True
tau2	89.3058333	200	50.0000000	100000.000	True
tau3	1207.19319	1000	50.0000000	100000.000	True
delta_sigma	175.605352	0	0.00000000	10000.0000	True
r	0.67069161	0.1	0.00000000	1.00000000	True
t_echo	17.0482631	17	14.0000000	19.0000000	True
delta_t	nan	-inf	-inf	inf	True

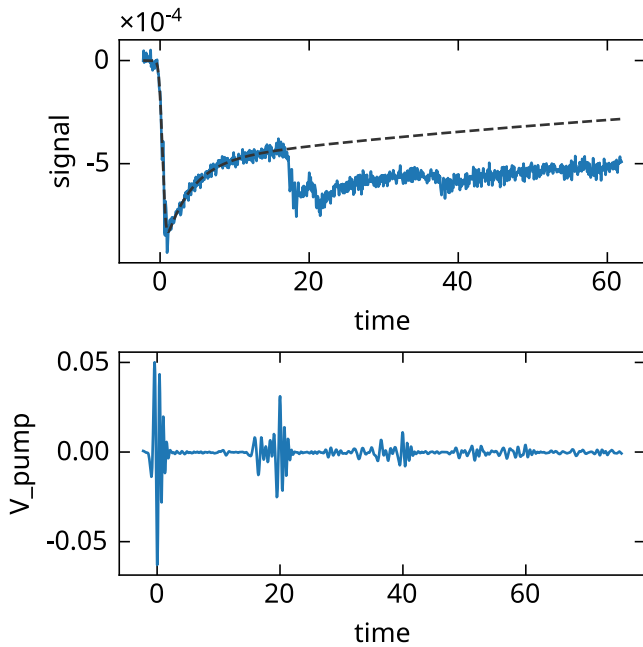


### 5.1.5 Paper plot



## 5.2 One-dimensional scans

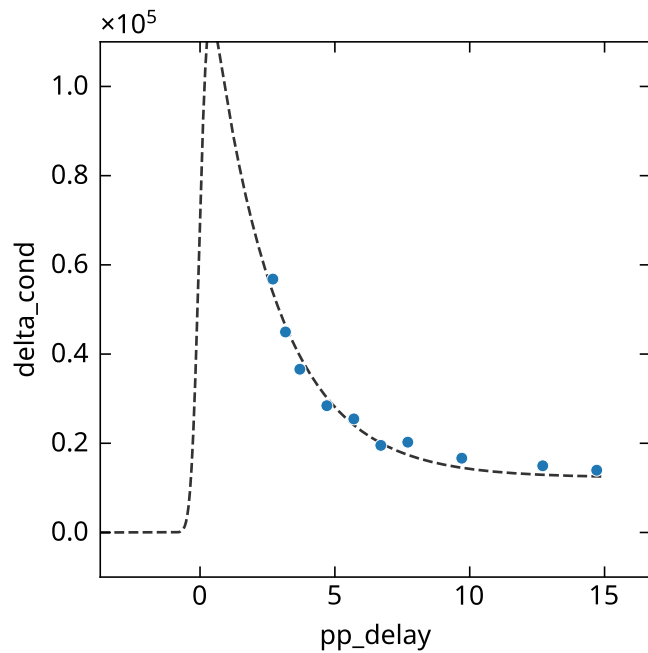
name	value	standard error	relative error	initial value	min	max	vary
t0	0.32986315	0.00660545	(2.00%)	0	-1.00000000	1.00000000	True
tau_fast	3.50437127	0.27979687	(7.98%)	1	0.00000000	10.00000000	True
tau_slow	110.262046	39.0150831	(35.38%)	100	0.00000000	1000.00000	True
amp_fast	-4.8011e-04	1.8975e-05	(3.95%)	-0.001	-0.010000000	0.000000000	True
amp_slow	-4.9664e-04	2.4921e-05	(5.02%)	-0.001	-0.010000000	0.000000000	True



(a)

Figure 5.1: Parameters

name	value	standard error	relative error	initial value	min	max	vary
t0	0.000000000	0.000000000		0	-1.000000000	1.000000000	False
tau_fast	2.38613703	0.54387642	(22.79%)	3	0.000000000	10.000000000	True
tau_slow	inf	0.000000000	(0.00%)	inf	100.0000000	inf	False
amp_fast	128522.191	41965.1063	(32.65%)	60000.0	1000.00000	1000000.00	True
amp_slow	12304.3147	858.826870	(6.98%)	20000.0	1000.00000	1000000.00	True



(a)

Figure 5.2: Parameters

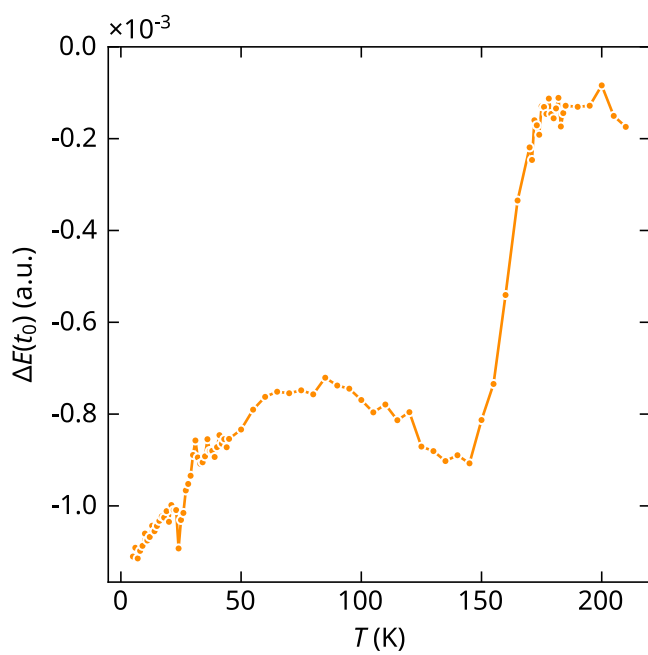


Figure 5.3: Temperature dependence of  $\Delta E$  at a fixed pump-probe delay of 13 ps.

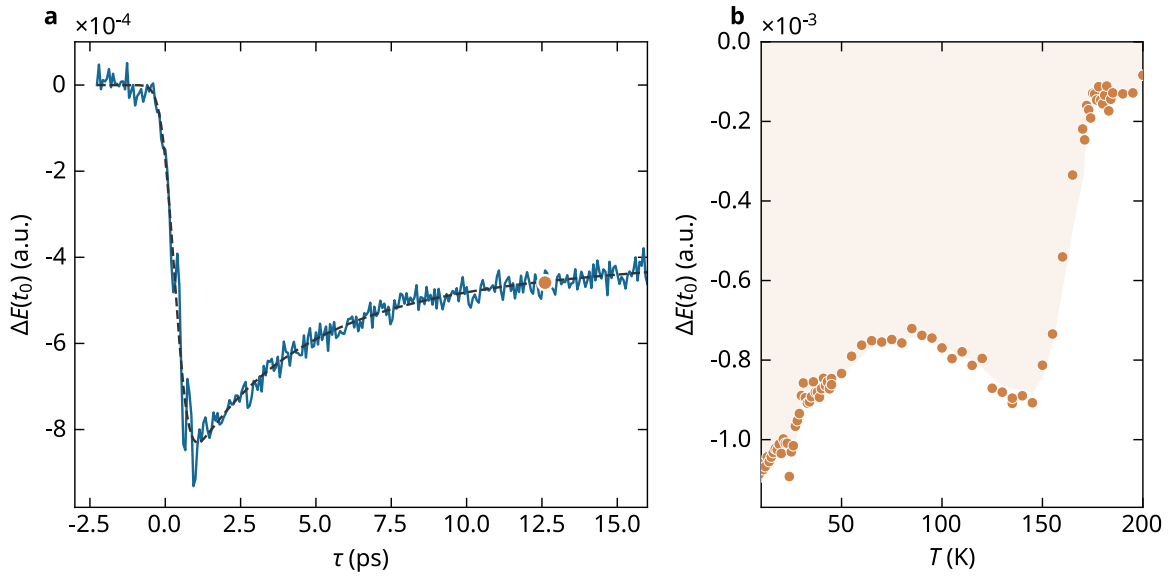


Figure 5.4: **a.** Decay dynamics with biexponential fit in black. The differential voltage  $\Delta V_{pr}$  on the photodiodes is proportional to the pump-induced change in the transmitted electric field of the probe, as measured at a single time slice on the probe waveform. **b** The photodiode voltage  $V_{pu}$  is proportional to the electric field of the incident pump pulse. **c** Temperature dependence of  $\Delta V_{pr}$  at a fixed pump-probe delay of 13 ps.

## **Part III**

# **Electric field susceptibility**

# 6 Temperature

## 6.1 Experiment

Waveforms transmitted through the sample is recorded for a set of temperatures and pump field strengths, with the aim of assessing the “optical susceptibility”, in the sense of how the material response to the pump field strength. In this experiment, the probe THz waveforms arrives *20 ps* after the THz pump pulse. The dataset is structured as follows:

field_strength f64	temperature i64	time f64	X f64	X_eq f64	dX f64
0.000534	5	-10.0	0.0	0.0	0.0
0.000534	5	-9.997	0.0	0.0	0.0
0.000534	5	-9.994	0.0	0.0	0.0
0.000534	5	-9.991	0.0	0.0	0.0
0.000534	5	-9.988	0.0	0.0	0.0
...	...	...	...	...	...
0.9584161	151	49.985	0.0	0.0	0.0
0.9584161	151	49.988	0.0	0.0	0.0
0.9584161	151	49.991	0.0	0.0	0.0
0.9584161	151	49.994	0.0	0.0	0.0
0.9584161	151	49.997	0.0	0.0	0.0

The raw signal  $X$  is the absolute waveforms, and  $dX$  is calculated by subtracting  $X_{eq}$ , which is defined as the waveform corresponding to zero pump field strength.

The time-domain data is transformed to the frequency domain. The measured signal is the differential signal (pump on minus pump off), and one trace of the absolute waveform absent pump. We therefore look at the relative transmission amplitude in the frequency domain, defined as

$$\hat{t}_r(\tau) \equiv \frac{\Delta \hat{t}}{\hat{t}_0} = \frac{\Delta \hat{S}(\tau)}{\hat{S}_0} \quad (6.1)$$

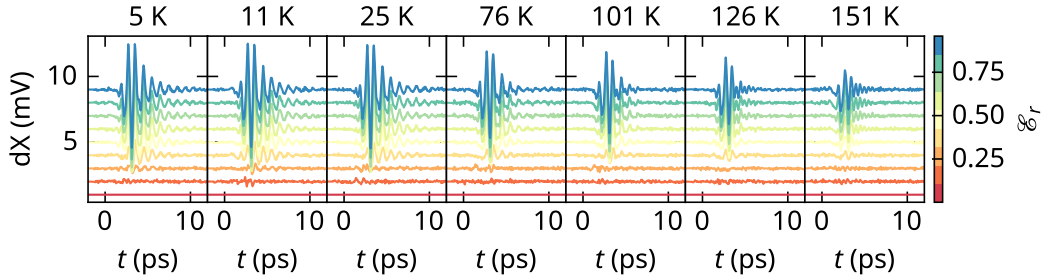


Figure 6.1: Summary of raw differential waveforms, recorded after transmission through the sample for various values of the THz pump field strength and sample temperature. In black, the equilibrium absolute waveform.

Here,  $\Delta\hat{S}$  is the discrete Fourier transform of “ $dX$ ”, and  $\hat{S}_0$  is the Fourier transform of the  $X_{eq}$ , the equilibrium waveform.  $T$  is the sample temperature, and  $\mathcal{E}_r$  the pump field strength (normalized, with unity corresponding to about 200 kV/cm).

## 6.2 Calculations

The transmission amplitude of the sample can be calculated theoretically, with the simplifying assumption that any field-induced variation in conductivity occurs exclusively in the capacitor-like gap of the split-ring resonator.

Aiming to map the theoretical resonator-gap conductivity  $\sigma$  to the experimental parameters  $T$  and  $\mathcal{E}_r$ , we need to choose the appropriate reference spectrum when calculating the *relative* transmission amplitude,

$$\hat{t}_r(\sigma_0 = \sigma_0(T)) = \frac{\Delta\hat{t}}{\hat{t}_0} = \frac{\hat{t}(\sigma, \sigma_0) - \hat{t}(\sigma = \sigma_0)}{\hat{t}(\sigma = \sigma_0)}$$

To do this, we need to make a choice for  $\sigma_0$ , which is different for each temperature, and possibly for each field-strength. If we assume it is independent of field strength (*viz.* the field only affects the material in the resonator gap), we can use the analysis of the linear spectroscopy data, where a correspondence between temperature and film conductivity was obtained, as shown in Figure 6.2.

Then we obtain  $\sigma(T, \mathcal{E}_r)$  by solving Equation 6.2, which we call the *fixed- $\sigma_0$  minimization*.

$$\min_{\sigma} \epsilon(T, \mathcal{E}_r; \sigma, \sigma_0) \Big|_{\sigma_0=\sigma_0(T)} \quad (6.2)$$

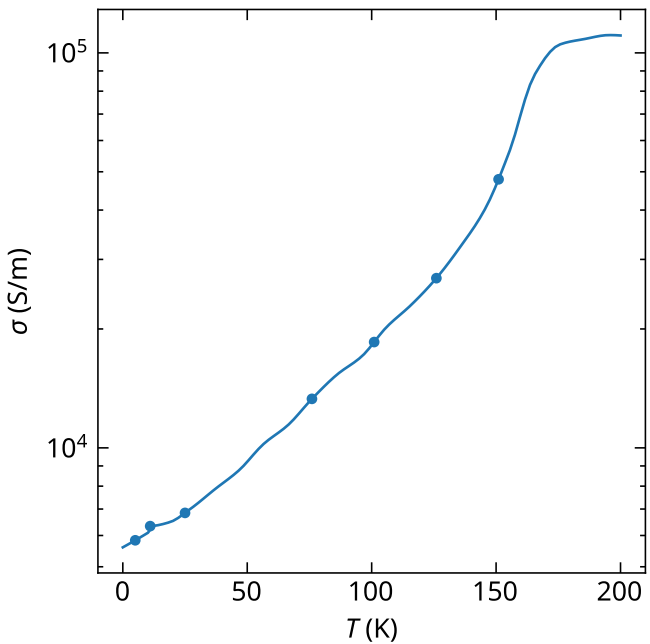


Figure 6.2: Summary of raw differential waveforms, recorded after transmission through the sample for various values of the THz pump field strength and sample temperature. In black, the equilibrium absolute waveform.

where

$$\epsilon(T, \mathcal{E}_r; \sigma, \sigma_0) = \sum_i |w(f_i) (\hat{t}_{r,\text{meas}}(f_i; T, \mathcal{E}_r) - \hat{t}_{r,\text{calc}}(f_i; \sigma, \sigma_0))|^2 \quad (6.3)$$

the weighted residual sum of squares, with  $w(f)$  a weighting function that peaks around the resonance frequency.

On the other hand, we can also solve for both the local resonator gap conductivity  $\sigma$  and the film conductivity  $\sigma_0$  in a bilevel minimization scheme, determining both  $\sigma$  and  $\sigma_0$  from the same experiment. This leaves two choices: either we assume, as we did in the *fixed- $\sigma_0$  minimization*, that  $\sigma_0 = \sigma_0(T)$ , and does not depend on field strength  $\mathcal{E}_r$ , or we allow  $\sigma_0$  to vary with  $\mathcal{E}_r$  as well. We call these the *rigid- $\sigma_0$  minimization* and the *free- $\sigma_0$  minimization*, respectively.

The *rigid- $\sigma_0$  minimization* is given by Equation 6.4,

$$\min_{\sigma_0} \left\langle \epsilon(T, \mathcal{E}_r; \sigma, \sigma_0) \right\rangle_{\sigma=\sigma^*} \quad \text{where} \quad \sigma^*(T, \mathcal{E}_r; \sigma_0) = \arg \min_{\sigma} \epsilon(T, \mathcal{E}_r; \sigma, \sigma_0) \quad (6.4)$$

where  $\langle \cdot \rangle_\alpha$  denotes the mean over variable  $\alpha$ . The *free- $\sigma_0$  minimization* is given by Equation 6.5,

$$\min_{\sigma_0} \epsilon(T, \mathcal{E}_r; \sigma, \sigma_0) \Big|_{\sigma=\sigma^*} \quad \text{where} \quad \sigma^*(T, \mathcal{E}_r; \sigma_0) = \arg \min_{\sigma} \epsilon(T, \mathcal{E}_r; \sigma, \sigma_0) \quad (6.5)$$

where the inner error is not averaged over  $\mathcal{E}_r$ . In Figure 6.3, we compare the results of these three minimization schemes.

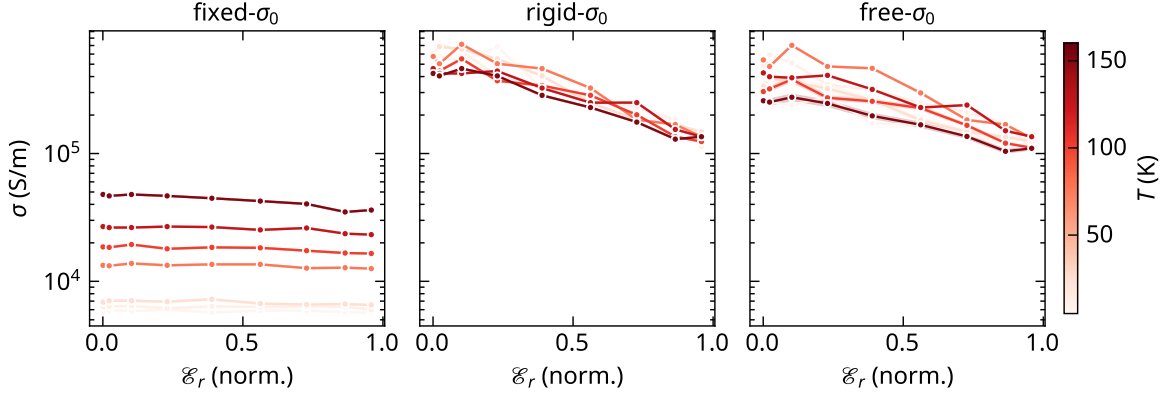


Figure 6.3: The resonator-gap conductivity as a function of field strength  $\mathcal{E}_r$  and temperature  $T$ , shown for each of the three minimization schemes.

The solutions are quite consistent with each other, giving the same trends while displaying some differences in absolute values. Henceforth, we will use the *fixed- $\sigma_0$  minimization*, as this ensures consistency with the linear spectroscopy data and with other analyses, and takes advantage of the high-quality solution of the linear spectroscopy experiment. We can look at this data as a function of temperature, for fixed field strengths, or as a function of field-strength, for fixed temperatures. These views are shown in Figure 6.4.

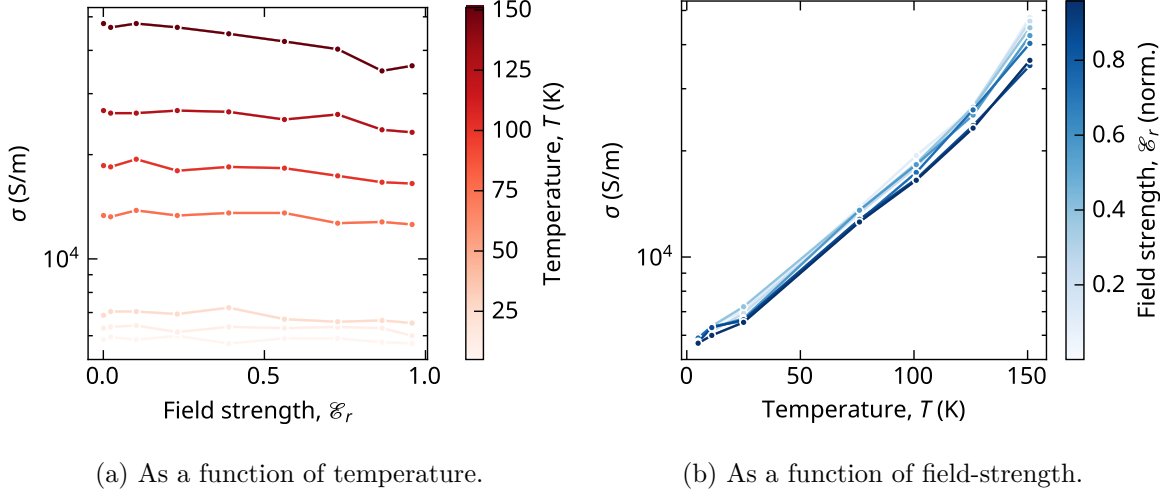


Figure 6.4: The temperature dependence of the resonator-gap conductivity  $\sigma$ , for a set of field strengths  $\mathcal{E}_r$ .

### 6.3 Field-assisted tunneling

The Landau-Dykne expression for the transition rate is

$$\Gamma = \frac{1}{2\pi} \exp\left(-\pi \frac{\mathcal{E}_0}{\mathcal{E}_r}\right)$$

If we take the conductivity to be proportional to this transition rate (which is a reasonable assumption, since the conductivity is proportional to the number of carriers), and we allow for a constant background conductivity  $\sigma_b$ , we can write the conductivity as

$$\sigma = \sigma_b + \sigma_{LD} \exp\left(-\frac{\pi \mathcal{E}_0}{\mathcal{E}_r}\right) \quad (6.6)$$

We can fit this model to the data, and evaluate the temperature dependence of the relative threshold field  $\mathcal{E}_0$ . The value of  $\sigma_{LD}$  can be determined from the linear spectroscopy data, so that it is not a free parameter.

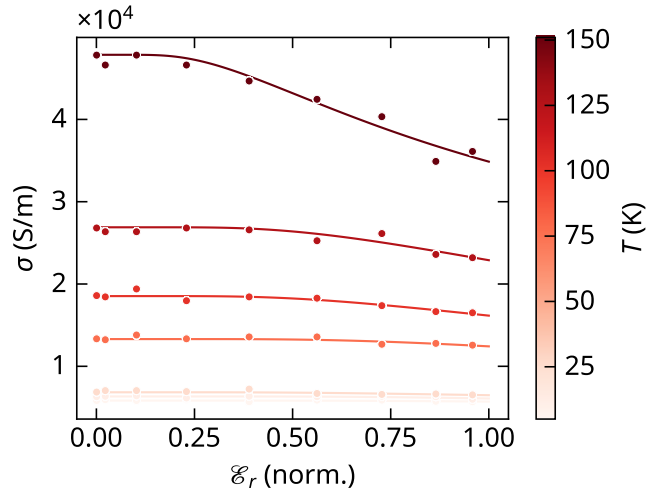


Figure 6.5: Landau-Dykhne fit to the resonator-gap conductivity  $\sigma$ , for a set of temperatures  $T$ .

The Landau-Dykhne model fits the data rather well, and yields the parameters  $\mathcal{E}_0$ , which is the (relative) field-strength threshold, and  $\sigma_0$ . This is shown in Figure 6.6.

A positive correlation between temperature and  $\mathcal{E}_0$  is surprising, and it should be considered whether this is physically realistic.

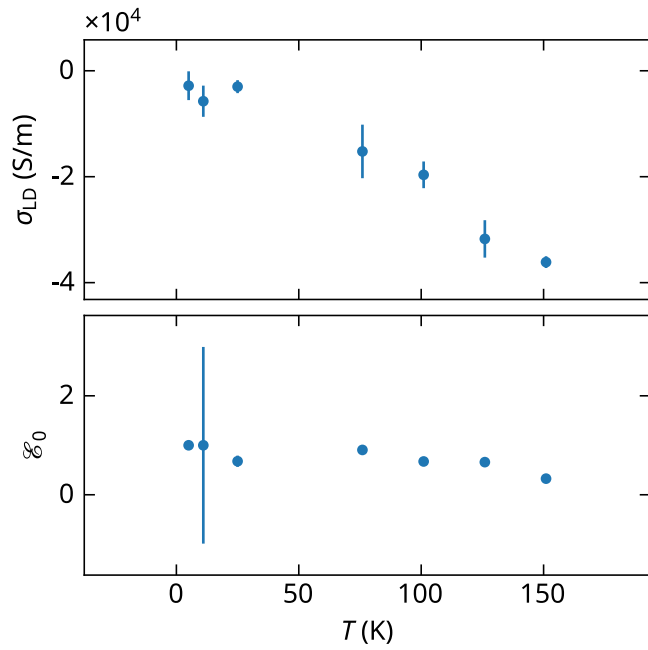


Figure 6.6: The field-strength threshold  $\mathcal{E}_0$  as a function of temperature  $T$ .

# 7 Nanosecond dynamics

## 7.1 Experiment

Waveforms transmitted through the sample is recorded over the parameter space constituted by the pump-probe delay (the common delay line of the optical gate and THz probe, with respect to the THz pump), and the pump field strength (controlled by a half-wave plate before the electro-optic crystal, which is followed by a polarizer).

We load the raw data from experiment, and pad with zeros to interpolate in the frequency domain. The dataset is structured as follows:

time f64	field_strength f64	pp_delay f64	X f64
-10.0	0.96	54.2938	0.0
-9.997	0.96	54.2938	0.0
-9.994	0.96	54.2938	0.0
-9.991	0.96	54.2938	0.0
-9.988	0.96	54.2938	0.0
...	...	...	...
49.985	0.87	37.118553	0.0
49.988	0.87	37.118553	0.0
49.991	0.87	37.118553	0.0
49.994	0.87	37.118553	0.0
49.997	0.87	37.118553	0.0

Figure Figure 8.1 shows the raw transmitted waveforms.

Next, we transform the time-traces to the frequency domain, and we consider the *relative* transmission amplitude to deconvolve the signal from the response function of the experimental apparatus (electro-optic crystal, mirrors, etc.). The relative transmission amplitude is defined as

$$\hat{t}_r(\tau, \mathcal{E}) \equiv \frac{\Delta \hat{t}}{\hat{t}_0} = \frac{\hat{S}(\tau, \mathcal{E}) - \hat{S}_0}{\hat{S}_0} \quad (7.1)$$

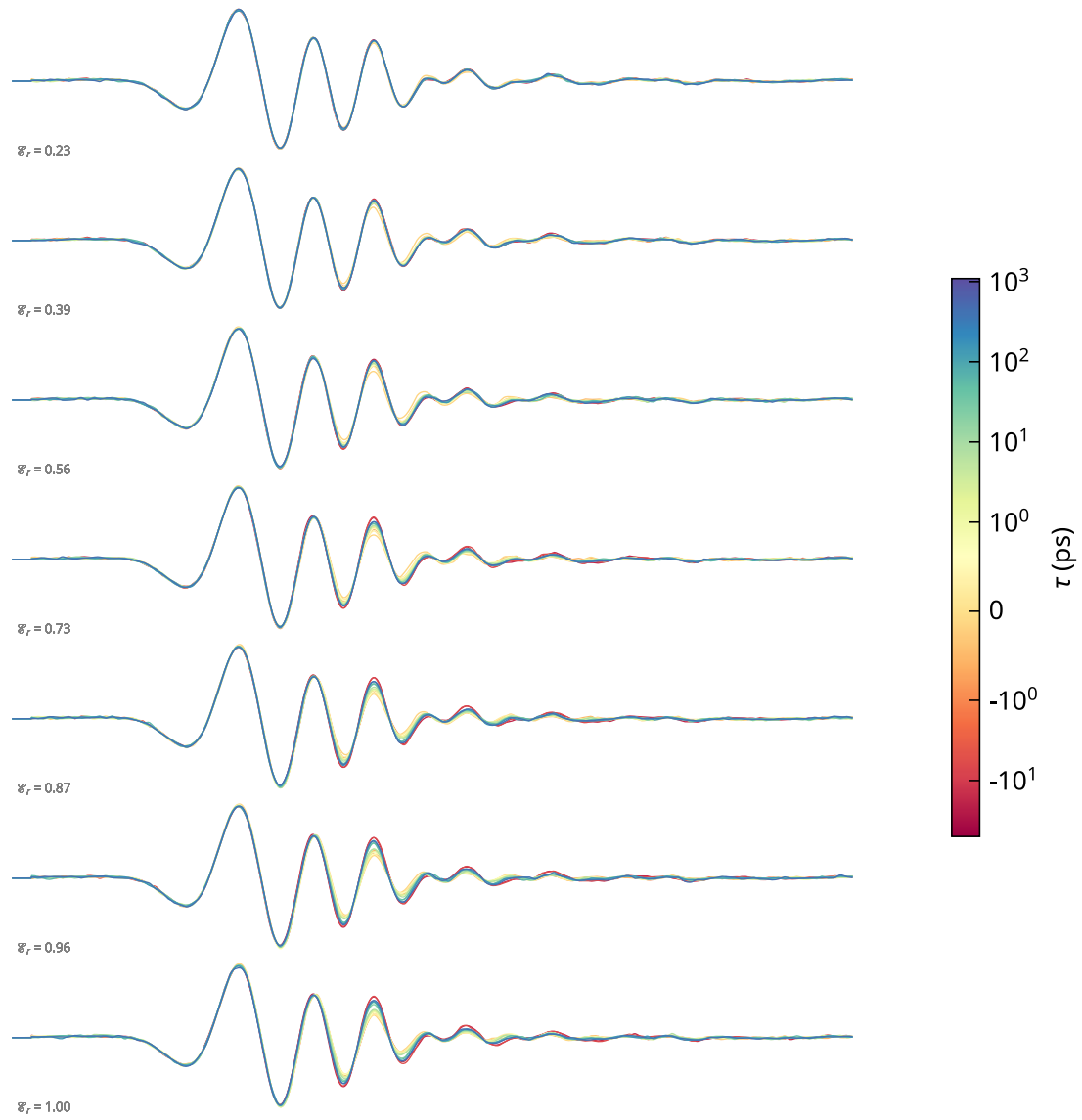


Figure 7.1: Summary of raw waveforms, recorded after transmission through the sample for various values of the THz pump field strength, and the pump-probe delay.

Here,  $\hat{S}$  is the discrete Fourier transform of a waveform,  $\tau$  is the pump-probe delay, and  $\mathcal{E}$  the relative pump field strength (unity corresponds to a peak electric field of about 200 kV/cm in the time domain). The dependence on frequency is omitted in the notation.  $\hat{S}_0$  represents the negative-delay ( $\tau < 0$ ) waveform, before the pump arrives, corresponding to the equilibrium signal.

field_strength f64	pp_delay f64	freq f64	t.reldiff.real f64	t.reldiff.imag f64
0.23	-49.8916	0.0	-0.682704	0.0
0.23	-49.8916	0.016667	-0.09978	-0.387496
0.23	-49.8916	0.033333	0.109525	-0.235633
0.23	-49.8916	0.05	0.203291	-0.137829
0.23	-49.8916	0.066667	0.303316	-0.054243
...	...	...	...	...
1.0	1090.6783	166.6	0.767381	-0.467309
1.0	1090.6783	166.616667	0.899228	-0.142229
1.0	1090.6783	166.633333	0.904498	0.028451
1.0	1090.6783	166.65	0.853525	0.252957
1.0	1090.6783	166.666667	-0.476353	0.0

## 7.2 Calculations

The calculated spectra are relativized with respect to the equilibrium spectrum,  $\hat{S}_0$ , which is the spectrum of the sample at the conductivity of the sample at the experimental temperature, determined in a separate experiment. This coincides with the negative-delay spectrum of the experiment, so that the reference spectra are the same for both measured and calculated relative transmission amplitudes.

cond_gap f64	cond_film f64	freq f64	t.reldiff.real f64	t.reldiff.imag f64
122.0	6458.79769	0.2	-0.000021	0.000016
122.0	6458.79769	0.256	0.00024	-0.000203
122.0	6458.79769	0.311	0.00001	-0.000032
122.0	6458.79769	0.366	-0.000022	-0.000021
122.0	6458.79769	0.42	-0.000027	0.000001
...	...	...	...	...
814000.0	6458.79769	2.063	-0.10965	-0.572256
814000.0	6458.79769	2.095	-0.041342	-0.531946
814000.0	6458.79769	2.129	0.01358	-0.489615

cond_gap	cond_film	freq	t.reldiff.real	t.reldiff.imag
f64	f64	f64	f64	f64
814000.0	6458.79769	2.165	0.062014	-0.447191
814000.0	6458.79769	2.203	0.101754	-0.400465

### 7.3 Extracting the resonator-gap conductivity $\sigma$

We map the experimental parameter space  $(\tau, \mathcal{E})$  to the computational one  $(\sigma)$  by minimizing the error function in Equation 8.2.

$$\epsilon(\tau, \mathcal{E}; \sigma, \sigma_0) = \sum_i |w(f_i) (\hat{t}_{r,\text{meas}}(f_i; \tau, \mathcal{E}) - \hat{t}_{r,\text{calc}}(f_i; \sigma, \sigma_0))|^2 \quad (7.2)$$

Here  $w$  is a weight that peaks around the resonance frequency, and tapers off at higher frequencies. In Figure 8.3 we show the logarithm of  $\epsilon$  for each combination of parameters, and we can identify a clear minimum for all combinations.

Selecting the least-error values for  $\sigma$ , we can plot the conductivity as a function of the pump-probe delay, shown in Figure 7.4.

cond_gap	cond_film	pp_delay	field_strength
f64	f64	f64	f64
6218.550422	6458.79769	-49.8916	0.39
11323.98959	6458.79769	10.005	0.39
13626.659608	6458.79769	15.0075	0.39
20260.659481	6458.79769	54.2938	0.56
16253.663369	6458.79769	10.005	0.56
...	...	...	...
6672.889012	6458.79769	-9.8716	1.0
24814.167462	6458.79769	274.4038	1.0
45990.295018	6458.79769	5.03585	0.87
63724.380796	6458.79769	54.2938	1.0
20803.569374	6458.79769	5.03585	0.56

It is instructive to consider the dependence on the relative pump field strength  $\mathcal{E}$  at various pump-probe delays  $\tau$ . This is shown in Figure 7.5.

The relationship looks exponential, so in Figure 7.5 we fit the data to the form in Equation 7.3, shown in solid lines.

$$\frac{\sigma(t)}{\sigma_0} = e^{\alpha \mathcal{E}(t=0)} \quad (7.3)$$

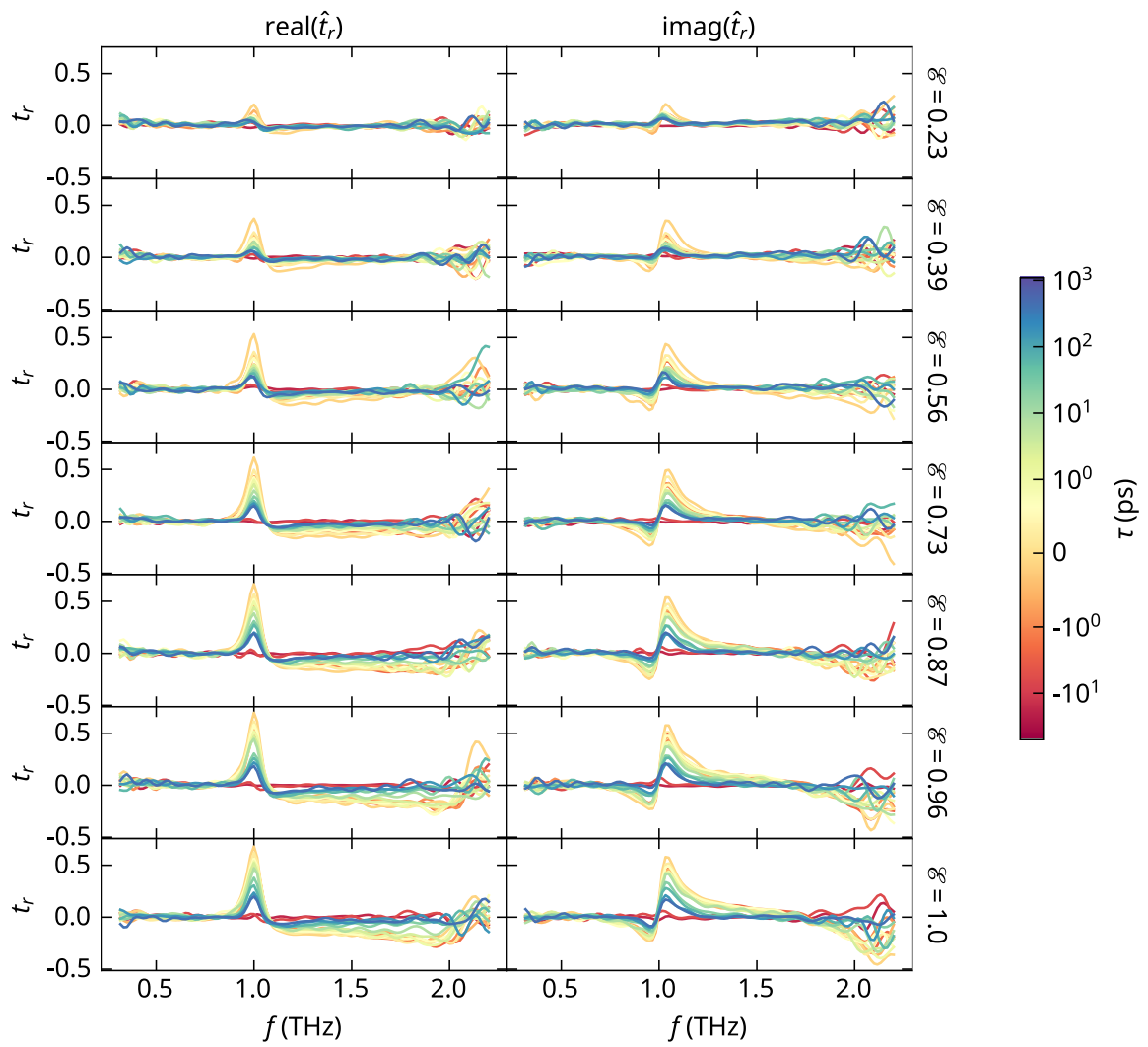


Figure 7.2: Relative transmission amplitude for measured spectra.

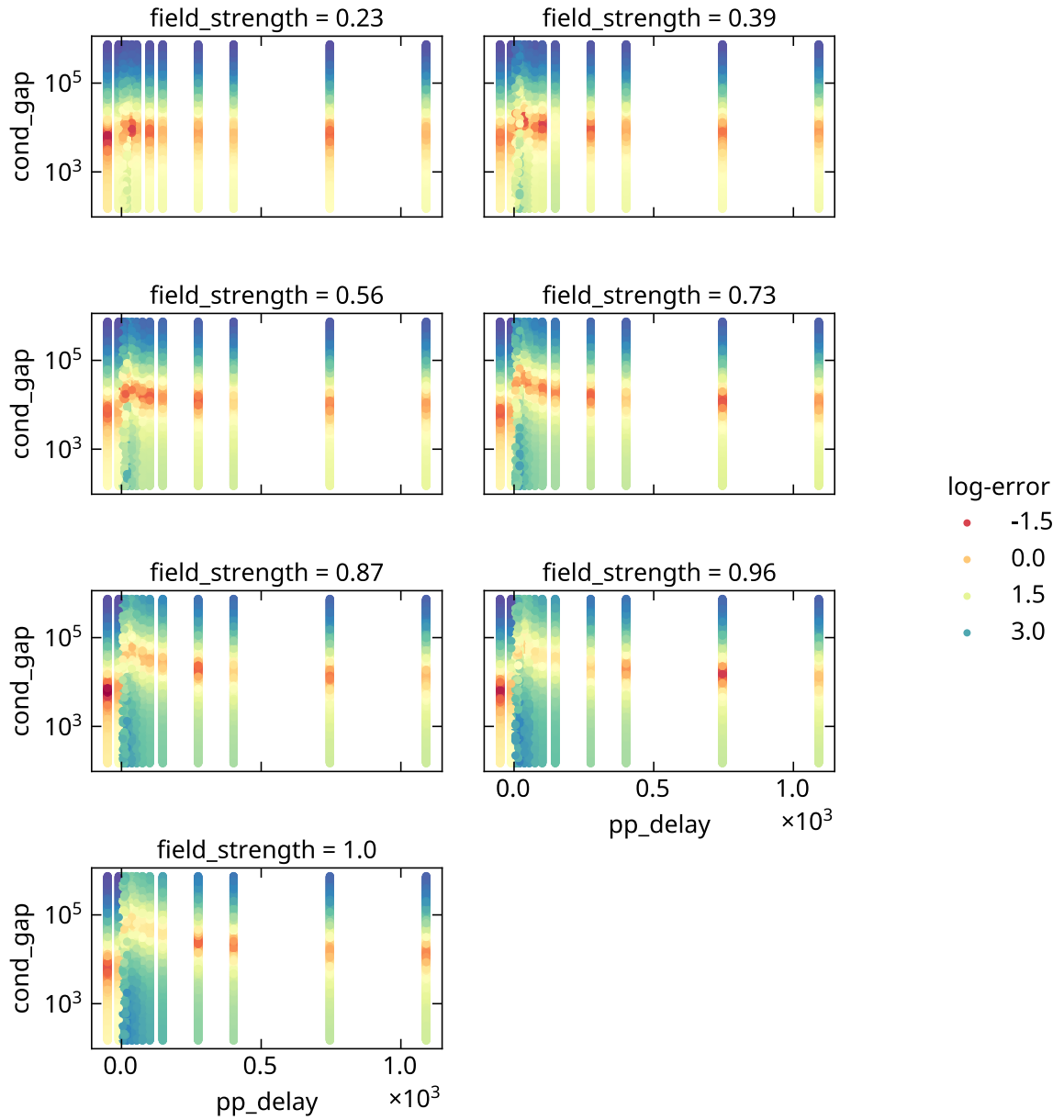


Figure 7.3: The residual sum of squares (RSS) for all pump-probe time-delays ( $\tau$ ) and relative field strengths ( $\mathcal{E}$ ).

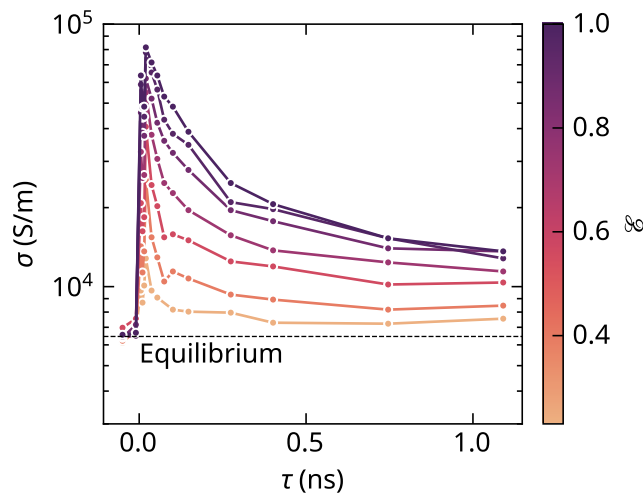


Figure 7.4: The time evolution of the resonator gap conductivity  $\sigma$ , for a set of relative field strengths  $\mathcal{E}$ .

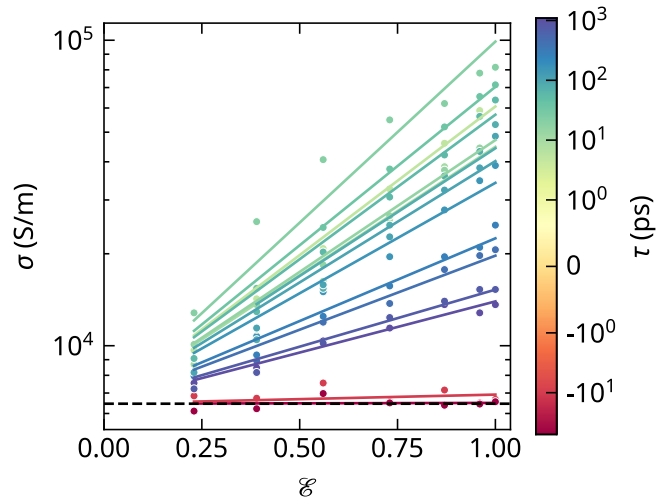


Figure 7.5: Field-strength dependence, at various pump-probe time delays  $\tau$ . Solid lines are fits to the exponential function, in Equation 7.3.

After fitting, we can then have a look at the time dependence,  $\alpha(\tau)$ , shown in Figure 7.6.

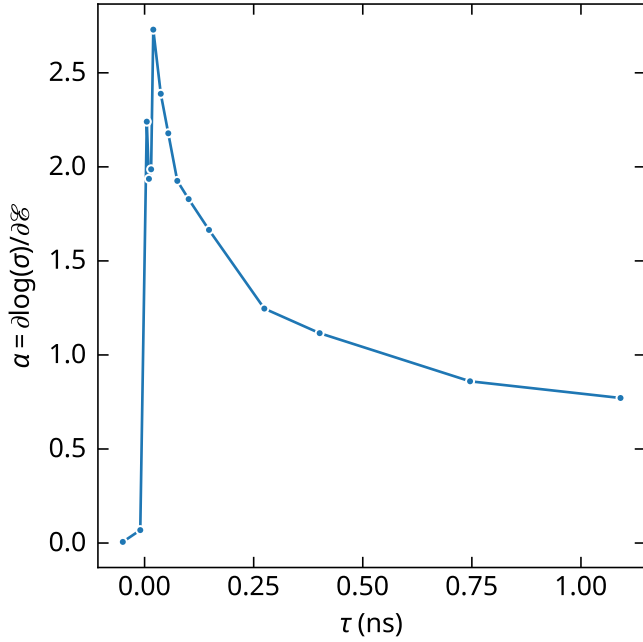


Figure 7.6: The exponential factor  $\alpha$  from Equation 7.3, as a function of the pump-probe delay  $\tau$ .

## 7.4 Timescales

Let us consider the decay dynamics of the conductivity, and a generic decay model of the form in Equation 7.4. The decay model is a sum of exponentials, with a step function  $\Theta(t - t_0)$  that accounts for the fact that the conductivity is zero before the pump pulse arrives. The parameters are the initial conductivity  $\sigma_0$ , the time  $t_0$  at which the pump pulse arrives, and the decay times  $\tau_i$  and amplitudes  $a_i$ . We include also a constant term  $a_0$ , which models an “infinite” lifetime component.

$$\sigma = \sigma_0 + \Theta(t - t_0) \left( a_0 + \sum_{i=1}^N a_i e^{-t/\tau_i} \right) \quad (7.4)$$

We first consider a single decay time ( $N = 1$ ), no infinite-lifetime component ( $a_0 = 0$ ), and  $t_0 = 0$ . The result is shown in Figure 7.7.

This is not a good fit, not least because there is a pump pulse echo at 20 ps, where the conductivity is raised further. We consider now  $t_0 = 20$ , measuring the decay time from the

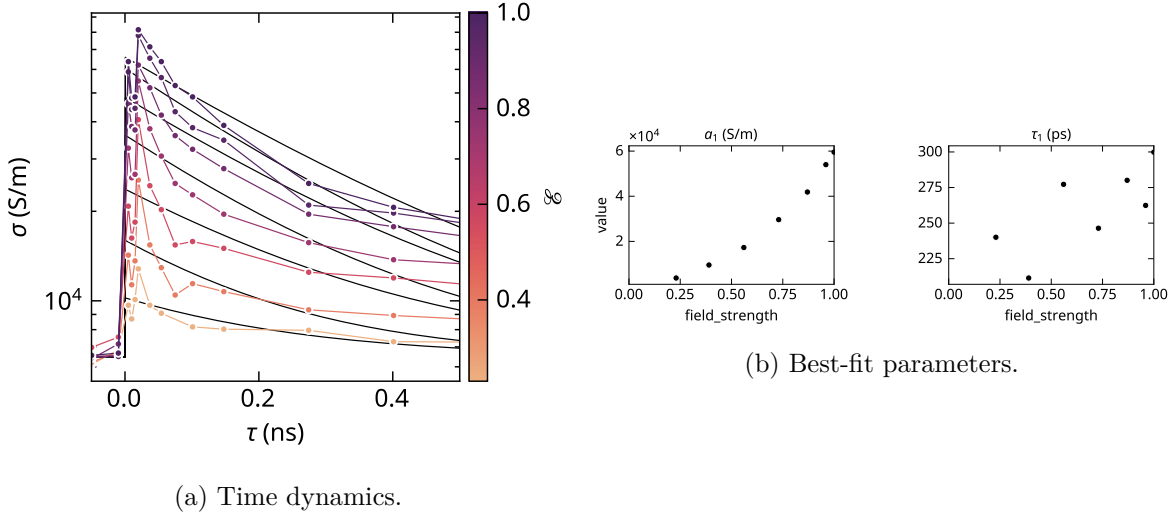


Figure 7.7: Fit to Equation 7.4 with single decay time ( $N = 1$ ), no infinite-lifetime component ( $a_0 = 0$ ), and  $t_0 = 0$ .

last pump pulse echo, where the conductivity is at its highest. We also include the infinite-lifetime component as a fit parameter. The result is shown in Figure 7.8.

Finally, we include a second decay time, and remove the infinite-lifetime component. This is shown in Figure 7.9.

This seems to match the data quite well. It looks like a single exponential decay is not sufficient to describe the dynamics, and a biexponential model is required. We take a closer look at the long-time behavior in Figure 7.10.

There is seeming inconsistency in the long-term behavior as a function of field-strength. We can try to include an infinite-lifetime component, as shown in Figure 7.11.

This seems to match the data very well, and the fit parameters show some trends, with the exception of the lowest-field trace, which does not fit well to any of the above-mentioned models.

### Takeaway

The conductivity dynamics following the second pump pulse is best described by a *biexponential decay* model, with the inclusion of an *infinite-lifetime component*.

- There is a fast decay process of 10–35 ps, which slows down with increasing field strength. Its amplitude is (sub-)linear in field strength.
- There is a slow decay process of 200–300 ps, with a quadratic field strength dependence.

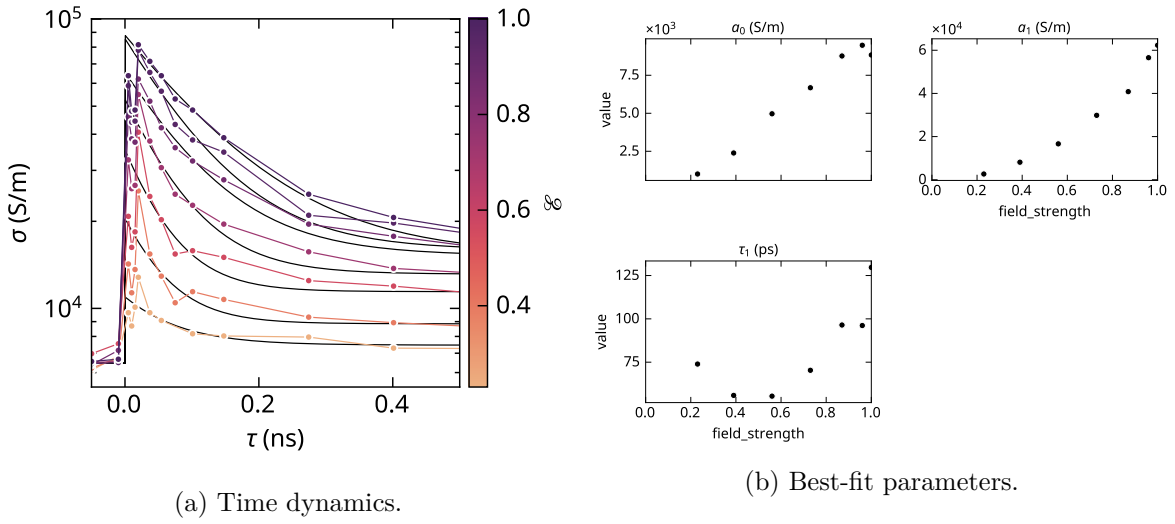


Figure 7.8: Fit to Equation 7.4 with single decay time ( $N = 1$ ), a free infinite-lifetime component ( $a_0 = 0$ ), and  $t_0 = 20$ .

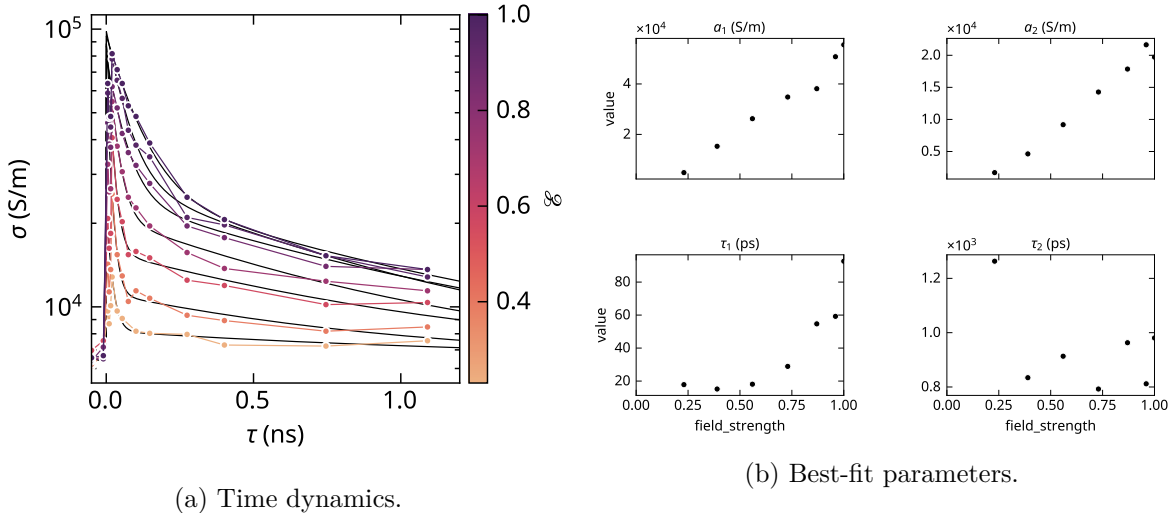


Figure 7.9: Fit to Equation 7.4 with two decay times ( $N = 2$ ), no infinite-lifetime component ( $a_0 = 0$ ), and  $t_0 = 20$ .

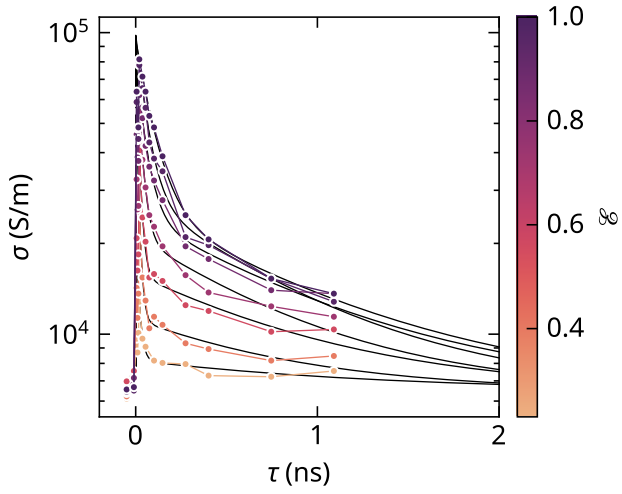


Figure 7.10: A look at the fit to Equation 7.4 with two decay times ( $N = 2$ ), no infinite-lifetime component ( $a_0 = 0$ ), and  $t_0 = 20$ , over long timescales.

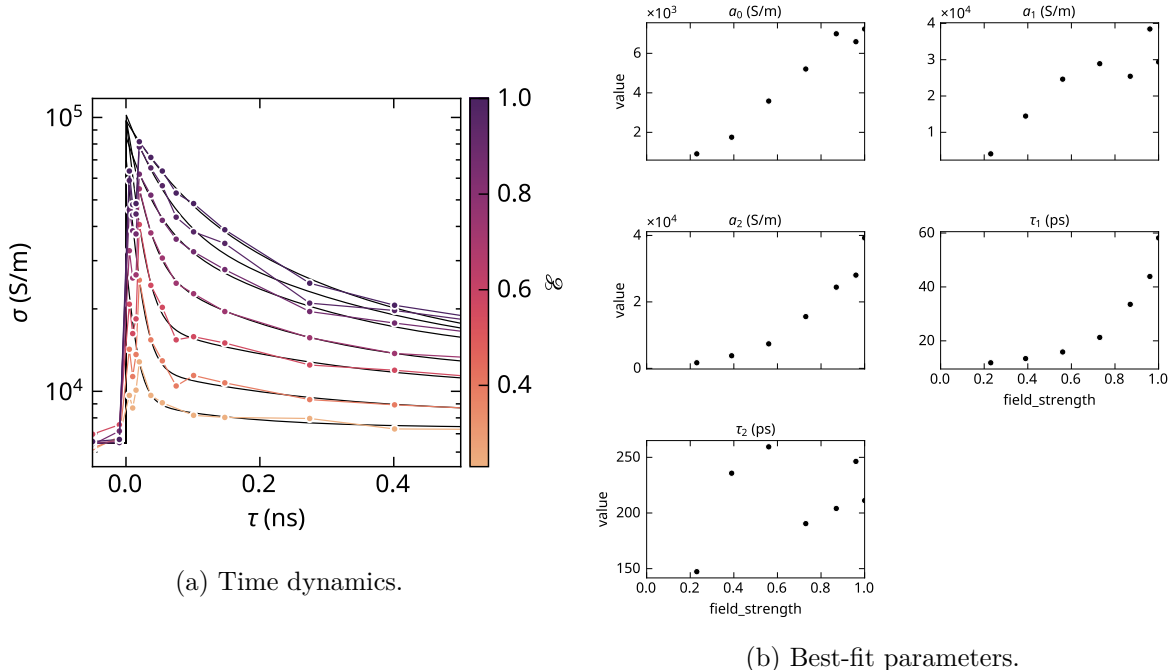


Figure 7.11: Fit to Equation 7.4 with two decay times ( $N = 2$ ), a free infinite-lifetime component ( $a_0 = 0$ ), and  $t_0 = 20$ .

- There is a remnant conductivity that persists for at least tens of nanoseconds, which increases linearly with field strength.

# 8 Detailed look at three timescales

## 8.1 Experiment

Waveforms transmitted through the sample is recorded over the parameter space constituted by the pump-probe delay (the common delay line of the optical gate and THz probe, with respect to the THz pump), and the pump field strength (controlled by a half-wave plate before the electro-optic crystal, which is followed by a polarizer), and the sample temperature. This analysis involves multiple experiments, taking place in the period 23-26 February 2023.

We load the raw data from experiment, and pad with zeros to interpolate in the frequency domain. The dataset is structured as follows:

dataset str	pp_delay f64	field_strength f64	temperature f64	time f64	X f64
"260223_xHWPfine"	0.0	0.133481	5.0	-10.0	0.0
"260223_xHWPfine"	0.0	0.133481	5.0	-9.997	0.0
"260223_xHWPfine"	0.0	0.133481	5.0	-9.994	0.0
"260223_xHWPfine"	0.0	0.133481	5.0	-9.991	0.0
"260223_xHWPfine"	0.0	0.133481	5.0	-9.988	0.0
...	...	...	...	...	...
"230223_xHWP_100ps_ProbeScan"	100.0	166.083134	5.0	49.985	0.0
"230223_xHWP_100ps_ProbeScan"	100.0	166.083134	5.0	49.988	0.0
"230223_xHWP_100ps_ProbeScan"	100.0	166.083134	5.0	49.991	0.0
"230223_xHWP_100ps_ProbeScan"	100.0	166.083134	5.0	49.994	0.0
"230223_xHWP_100ps_ProbeScan"	100.0	166.083134	5.0	49.997	0.0

Figure Figure 8.1 shows the raw transmitted waveforms.

Next, we transform the time-traces to the frequency domain, and we consider the *relative* transmission amplitude to deconvolve the signal from the response function of the experimental apparatus (electro-optic crystal, mirrors, etc.). The relative transmission amplitude is defined as

$$\hat{t}_r(\tau, \mathcal{E}) \equiv \frac{\Delta \hat{t}}{\hat{t}_0} = \frac{\hat{S}(\tau, \mathcal{E}) - \hat{S}_0}{\hat{S}_0} \quad (8.1)$$

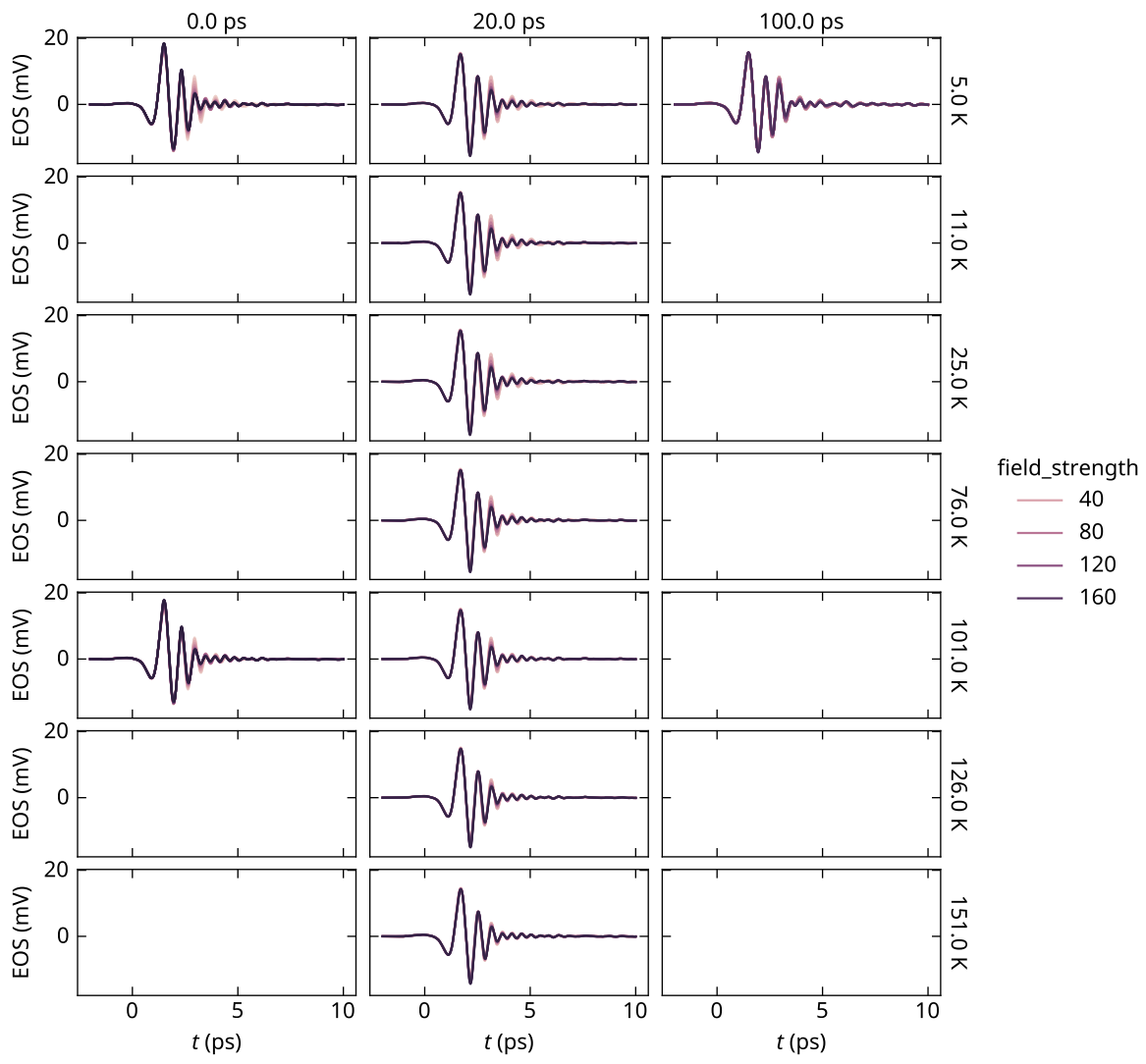


Figure 8.1: Summary of raw waveforms, recorded after transmission through the sample for various values of the THz pump field strength, and the pump-probe delay.

Here,  $\hat{S}$  is the discrete Fourier transform of a waveform,  $\tau$  is the pump-probe delay, and  $\mathcal{E}$  the pump field strength (unity corresponds to a peak electric field of about 200 kV/cm in the time domain). The dependence on frequency is omitted in the notation.  $\hat{S}_0$  represents waveform with  $\mathcal{E} = 0$ .

dataset str	pp_delay f64	field_strength f64	temperature f64	freq f64	t.reldiff.real f64	t.r f64
"230223_xHWP_100ps_ProbeScan"	100.0	0.006224	5.0	0.116667	0.0	-0.
"230223_xHWP_100ps_ProbeScan"	100.0	0.006224	5.0	0.133333	-0.0	-0.
"230223_xHWP_100ps_ProbeScan"	100.0	0.006224	5.0	0.15	0.0	0.0
"230223_xHWP_100ps_ProbeScan"	100.0	0.006224	5.0	0.166667	0.0	-0.
"230223_xHWP_100ps_ProbeScan"	100.0	0.006224	5.0	0.183333	0.0	-0.
...	...	...	...	...	...	...
"240223_xHWPxT"	20.0	184.015897	151.0	2.233333	0.131715	-0.
"240223_xHWPxT"	20.0	184.015897	151.0	2.25	0.211451	-0.
"240223_xHWPxT"	20.0	184.015897	151.0	2.266667	0.280469	-0.
"240223_xHWPxT"	20.0	184.015897	151.0	2.283333	0.330435	-0.
"240223_xHWPxT"	20.0	184.015897	151.0	2.3	0.35691	-0.

## 8.2 Calculations

The calculated spectra are relativized with respect to the equilibrium spectrum,  $\hat{S}_0$ , which is the spectrum of the sample at the conductivity of the sample at the experimental temperature, determined in a separate experiment. This coincides with the  $\mathcal{E} = 0$  spectra of the experiment, so that the reference spectra are the same for both measured and calculated relative transmission amplitudes.

## 8.3 Mapping

To extract the resonator-gap conductivity  $\sigma$  as a function of experimental parameters (the pump-probe delay  $\tau$ , the pump field strength  $\mathcal{E}$ , and the temperature  $T$ ), we minimize the following error (see Equation 8.2):

$$\epsilon(T, \mathcal{E}, \tau; \sigma) = \sum_i |w(f_i) (\hat{t}_{r,\text{meas}}(f_i; T, \mathcal{E}, \tau) - \hat{t}_{r,\text{calc}}(f_i; \sigma))|^2 \quad (8.2)$$

Here  $w$  is a weight that peaks around the resonance frequency. We verify in Figure 8.3 that each experimental configuration has a global minimum in the error.

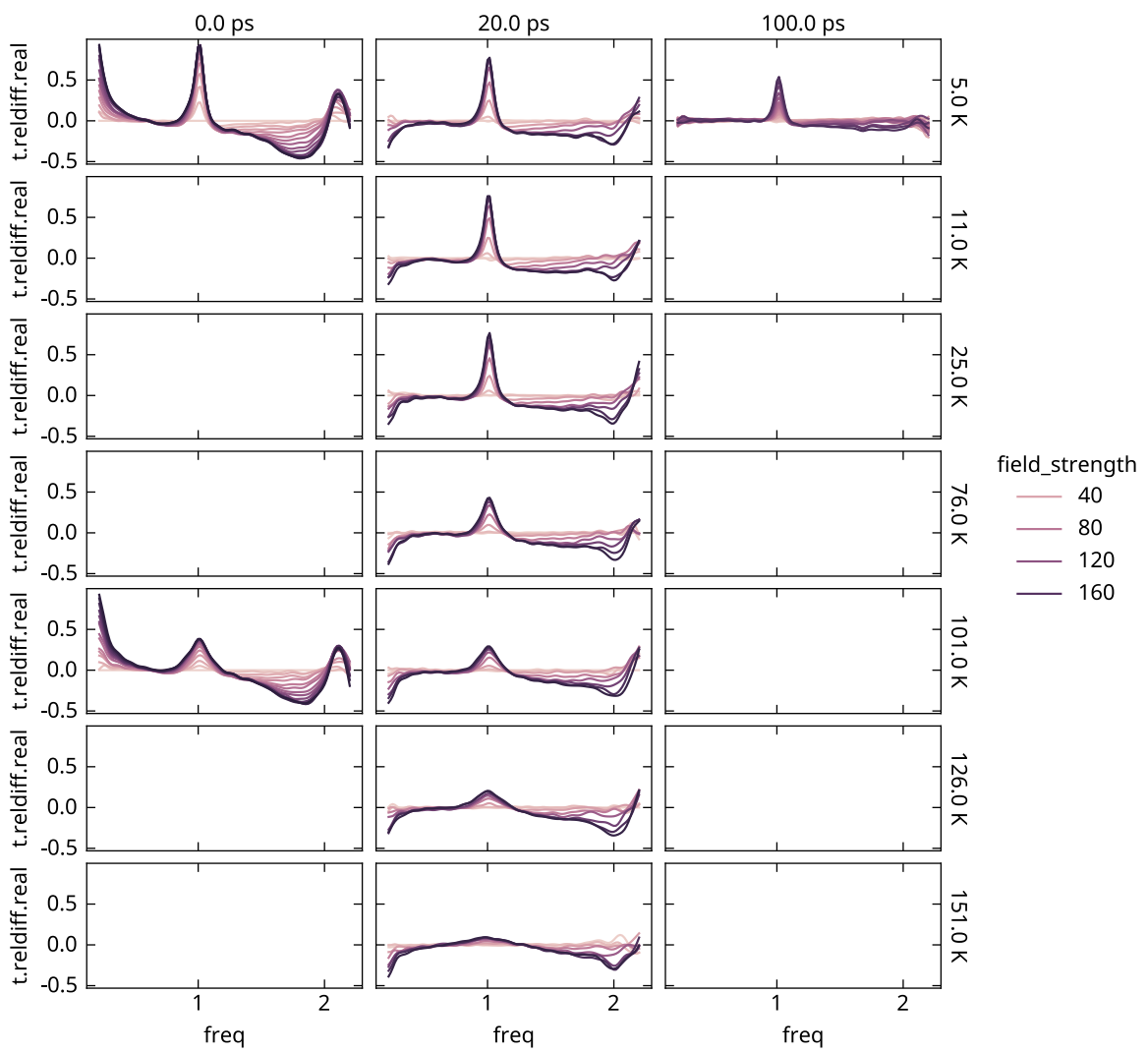


Figure 8.2: Relative transmission amplitude.

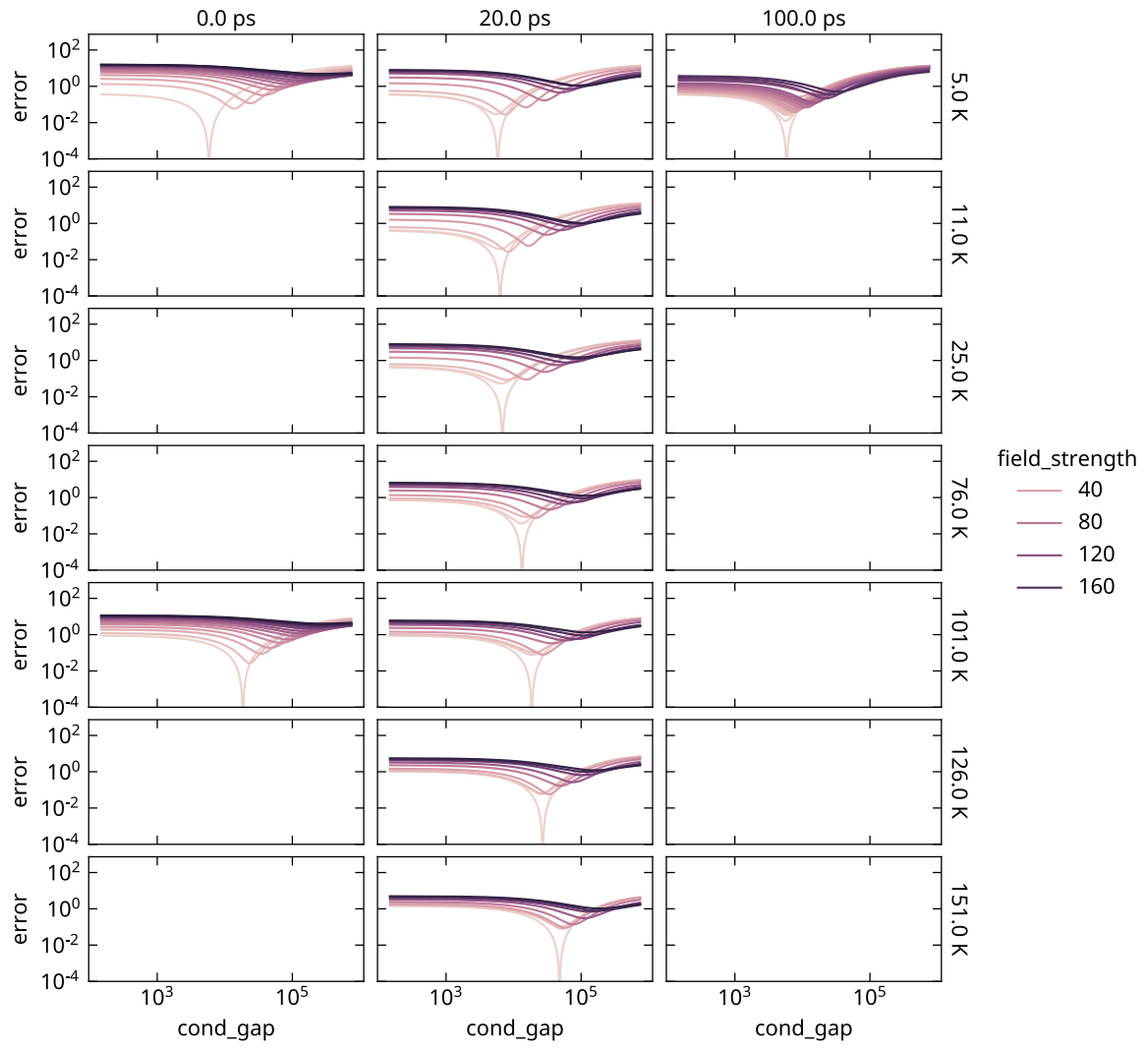
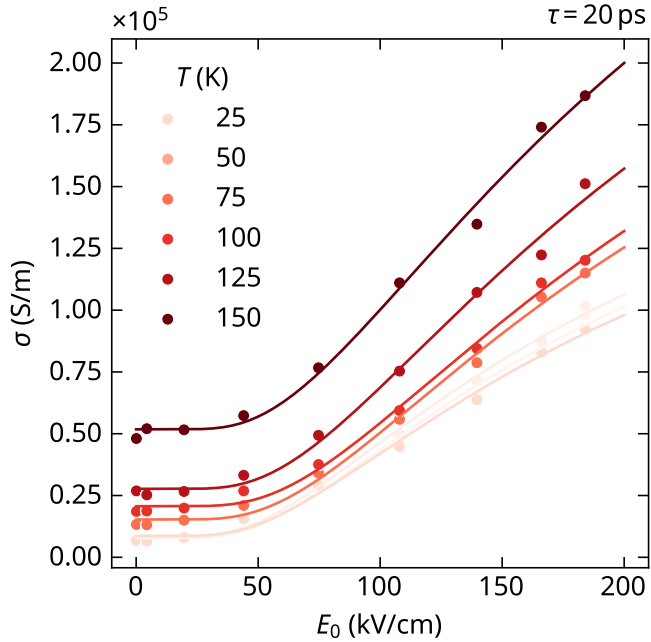


Figure 8.3: The residual sum of squares (RSS) for all pump-probe time-delays ( $\tau$ ), relative field strengths ( $\mathcal{E}$ ), and temperatures ( $T$ ).

Selecting the least-error values for  $\sigma$ , we can plot the conductivity as a function of the experimental parameters, shown in Figure 8.4.



We take an extra look at the lowest temperature, considering only the field-strength and pump-probe delay dependence, shown in Figure 8.5.

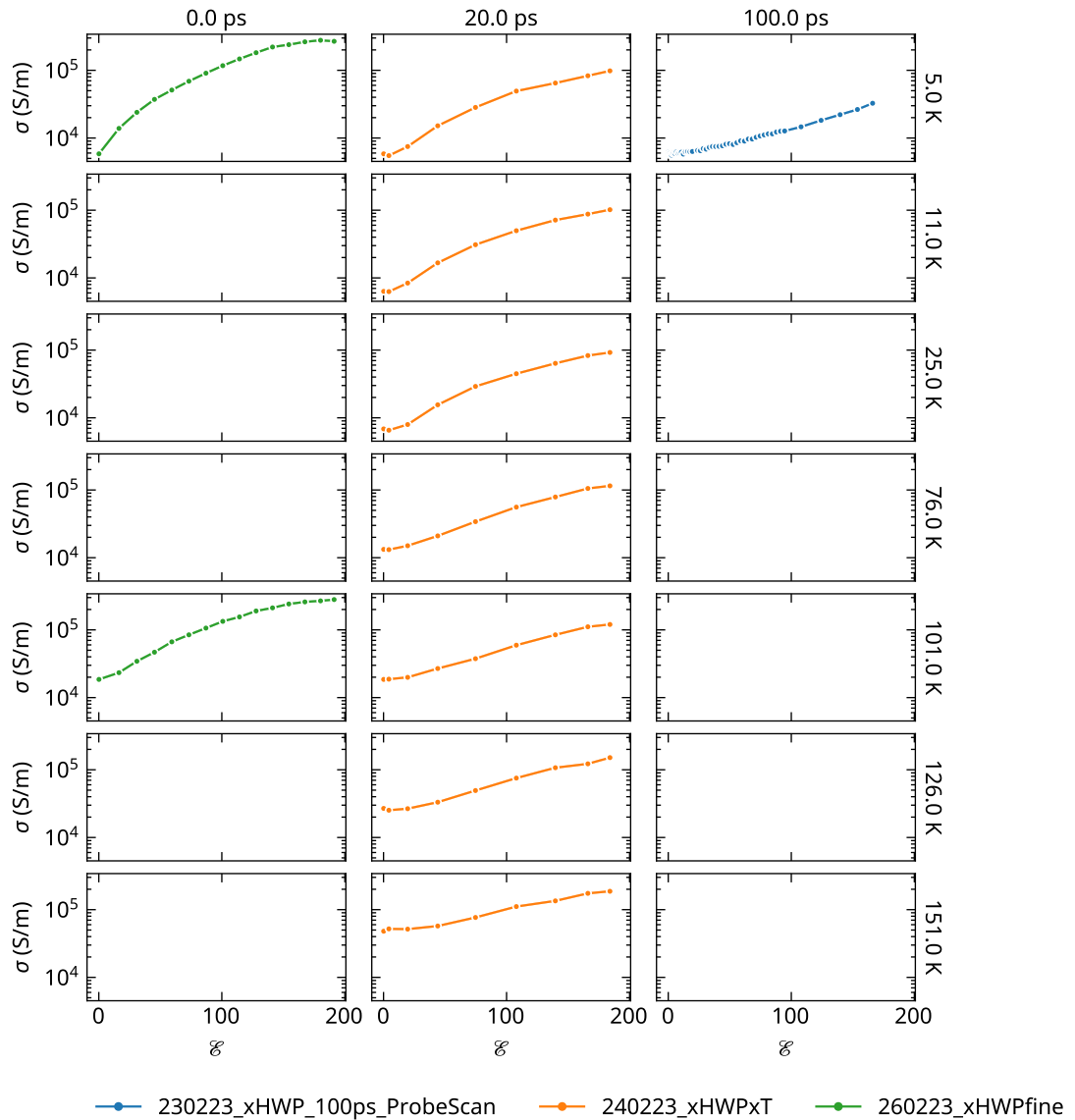


Figure 8.4: The time evolution of the resonator gap conductivity  $\sigma$ , for a set of field strengths  $\epsilon$ .

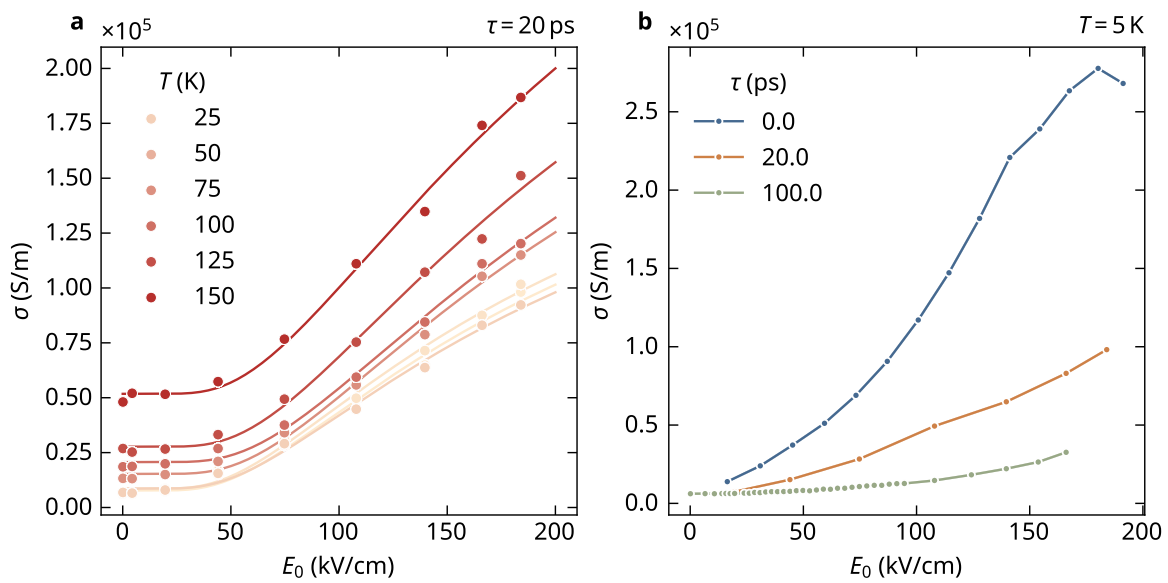


Figure 8.5: The time evolution of the resonator gap conductivity  $\sigma$ , for a set of field strengths  $\mathcal{E}$ .

# **Part IV**

# **Photodoping**

## 9 Photodoping a film

fluence f64	time f64	dX f64	X f64
0.379177	-5.0	0.0	0.0
0.379177	-4.994	0.0	0.0
0.379177	-4.988	0.0	0.0
0.379177	-4.982	0.0	0.0
0.379177	-4.976	0.0	0.0
...	...	...	...
0.482588	19.972	0.0	0.0
0.482588	19.978	0.0	0.0
0.482588	19.984	0.0	0.0
0.482588	19.99	0.0	0.0
0.482588	19.996	0.0	0.0

In order to obtain the complex conductivity, we make use of the following thin film approximation:

$$\Delta\sigma = -\frac{2}{Z_0 d} \frac{\Delta\hat{S}}{\hat{S} + \Delta\hat{S}} \quad (9.1)$$

Here  $\hat{S}$  denotes the Fourier transform of the electric waveform  $E(t)$ , and  $\Delta\hat{S}$  denotes the Fourier transform of the electro-optic differential waveform  $\Delta E(t)$ .

fluence f64	freq f64	X.real f64	X.imag f64	dX.real f64	dX.imag f64	t.reldiff.real f64	t.reldiff.imag f64	dsig.real f64
0.379177	0.0	0.000679	0.0	0.001764	0.0	2.595491	0.0	319130.795
0.379177	0.039997	-0.001741	-0.010737	-0.000517	-0.0011	0.107463	0.030727	43205.0198
0.379177	0.079994	0.00385	0.009598	-0.000026	-0.000243	-0.022761	0.00646	-10277.037
0.379177	0.11999	-0.012073	0.015107	-0.001796	0.000657	0.08453	-0.051317	35367.6763
0.379177	0.159987	0.068123	-0.020098	0.0033	0.001467	0.038718	-0.032953	16906.4192
...	...	...	...	...	...	...	...	...
0.482588	83.153348	0.000088	0.000046	-0.000012	0.000021	-0.008482	-0.241701	21227.0920

fluence f64	freq f64	X.real f64	X.imag f64	dX.real f64	dX.imag f64	t.reldiff.real f64	t.reldiff.imag f64	dsig.real f64
0.482588	83.193345	0.000025	0.00004	0.000021	-0.000003	0.172239	0.418674	107621.515
0.482588	83.233341	0.000008	-0.000089	0.000004	0.000006	-0.061753	-0.051856	-27662.273
0.482588	83.273338	0.00004	-0.00005	0.000005	-0.000027	0.379876	0.195685	128021.437
0.482588	83.313335	-0.000075	0.000021	-0.000014	0.000007	0.189797	0.038678	70914.2220

We know the initial conductivity from separate measurements, so that we can calculate the final conductivity as a function of fluence  $F$ , i.e.  $\sigma(F) = \sigma_0 + \Delta\sigma(F)$ . The full conductivity in the detectable frequency band is shown in Figure 9.2.

In Figure 9.3 the average conductivity within the experimental frequency band is shown as a function of pump fluence. Extrapolating, it appears that the full metallic state can be reached by pumping at a fluence of around  $1\text{ mJ/cm}^2$ . We are looking for the number of absorbed photons this corresponds to.

The (pseudocubic) unit cell area is  $a^2 \approx 0.16\text{ nm}^2$ , and there are 30 unit cells in the film thickness direction. That means the number of unit cells in the excited region is

$$N_{\text{uc}} = 30 \times A_{\text{ex}}/a^2 \approx 1.3 \times 10^{15}$$

The average number of photons in the pulse is

$$N_{\text{ph}} = E_{\text{pulse}}/\hbar\omega \approx 6.5 \times 10^{16}$$

where the energy of the pulse is

$$E_{\text{pulse}} = 1.0\text{ mJ/cm}^2 \times 7\text{ mm}^2 = 6.2 \times 10^{16}\text{ eV}$$

and the average photon energy is  $\hbar\omega = 0.95\text{ eV}$ . The number of photons per unit cell is therefore

$$N_{\text{ph}}/N_{\text{uc}} \approx 50$$

However, only a fraction of the photons are absorbed. The fraction of the pulse that is absorbed is

$$1 - (1 - R)e^{-d/\delta} \approx 0.3$$

where we used  $R = 0.3$ , based on measurements by T. Katsufuji et al.

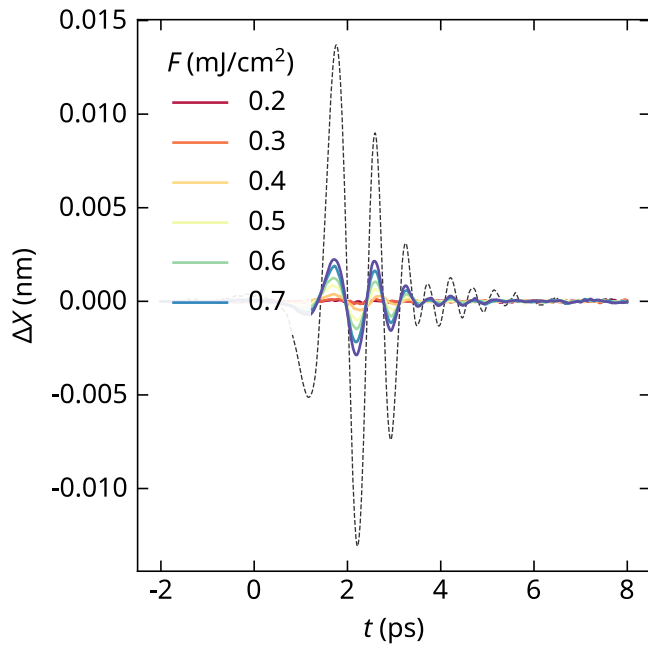


Figure 9.1: The transmitted electro-optic differential signal (pump-induced deformation of the probe waveforms) for a set of pump fluences. The pump wavelength is 1300 nm. The black dotted line corresponds to the absolute signal of the probe waveform, absent any pump.

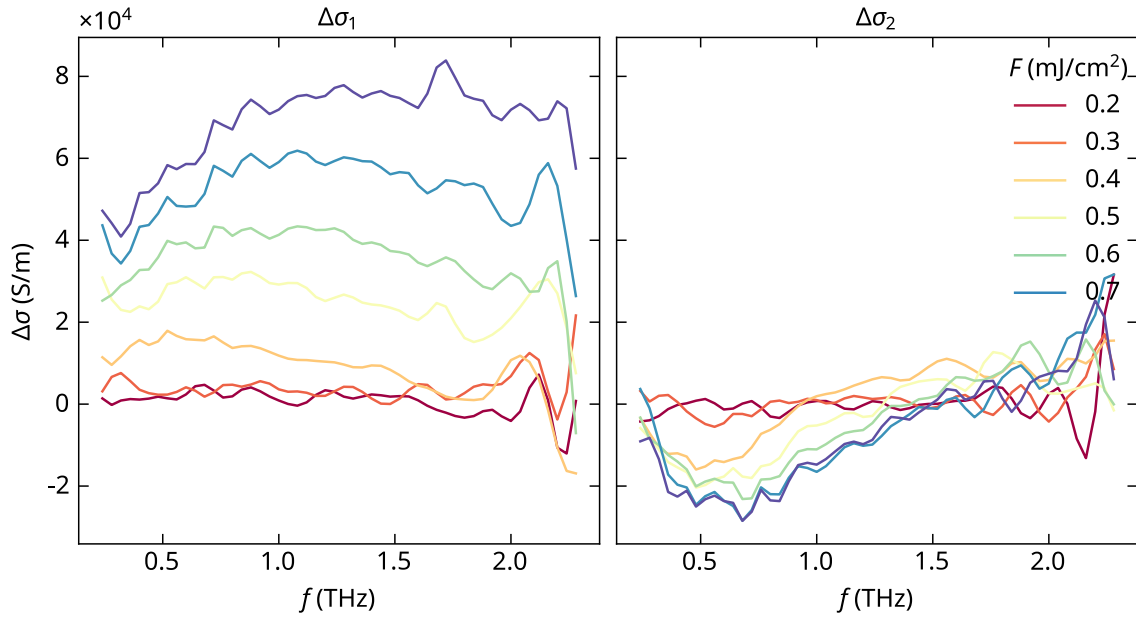


Figure 9.2: The real part of the terahertz conductivity,  $\sigma_1$ , as a function of frequency for a set of pump fluences.

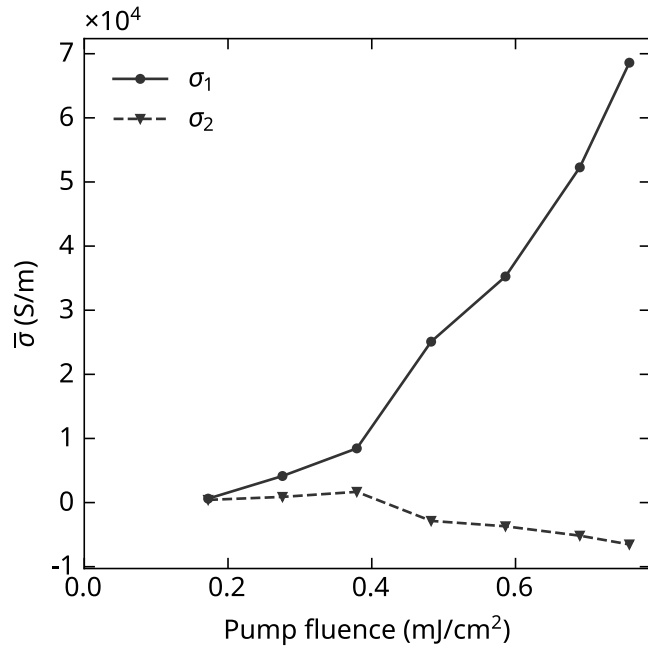
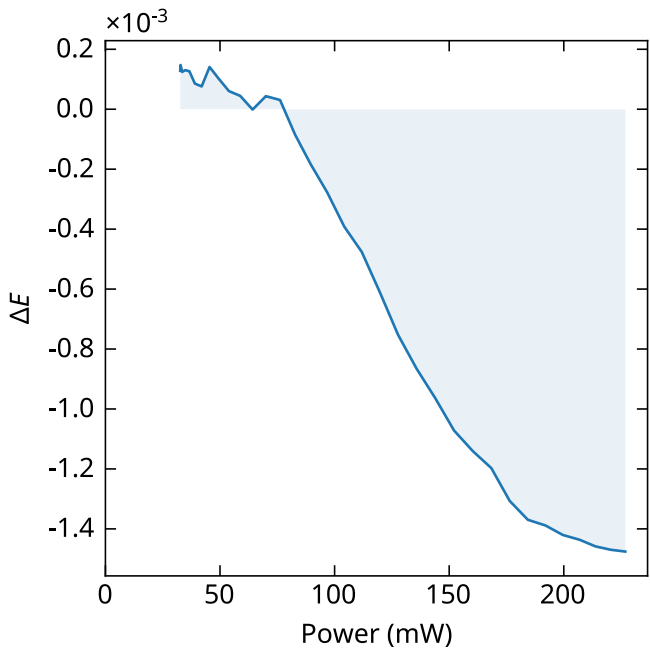
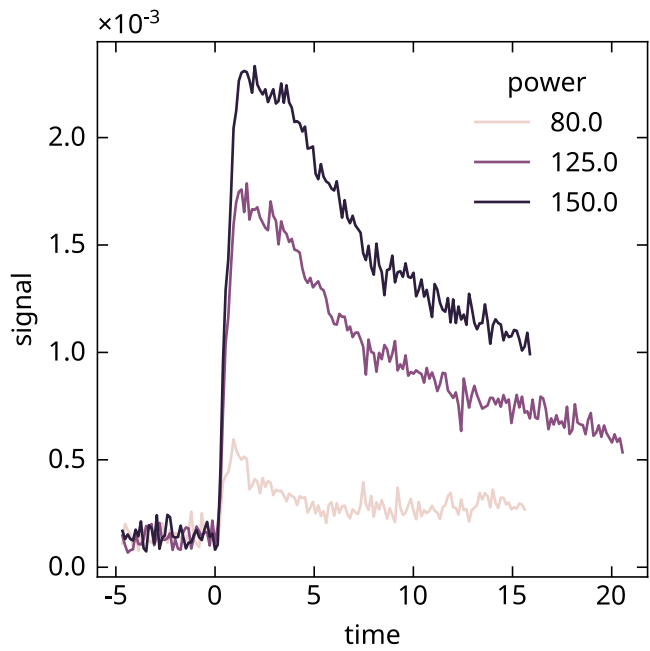
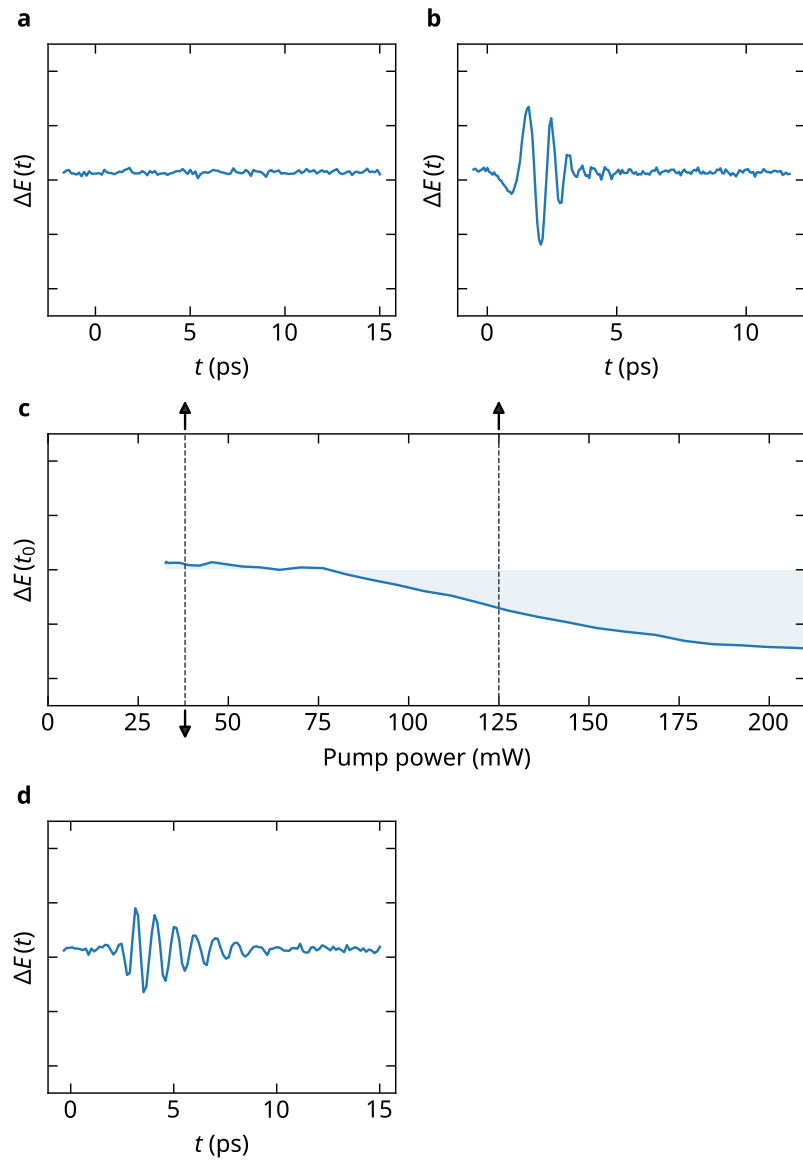


Figure 9.3: The average terahertz conductivity as a function of pump fluence. The black dotted lines correspond to the film conductivity at 4.40 K (bottom) and 200 K (top).

252782465726.74088  
3.503157894736842e-05



## 9.1 Sample comparison



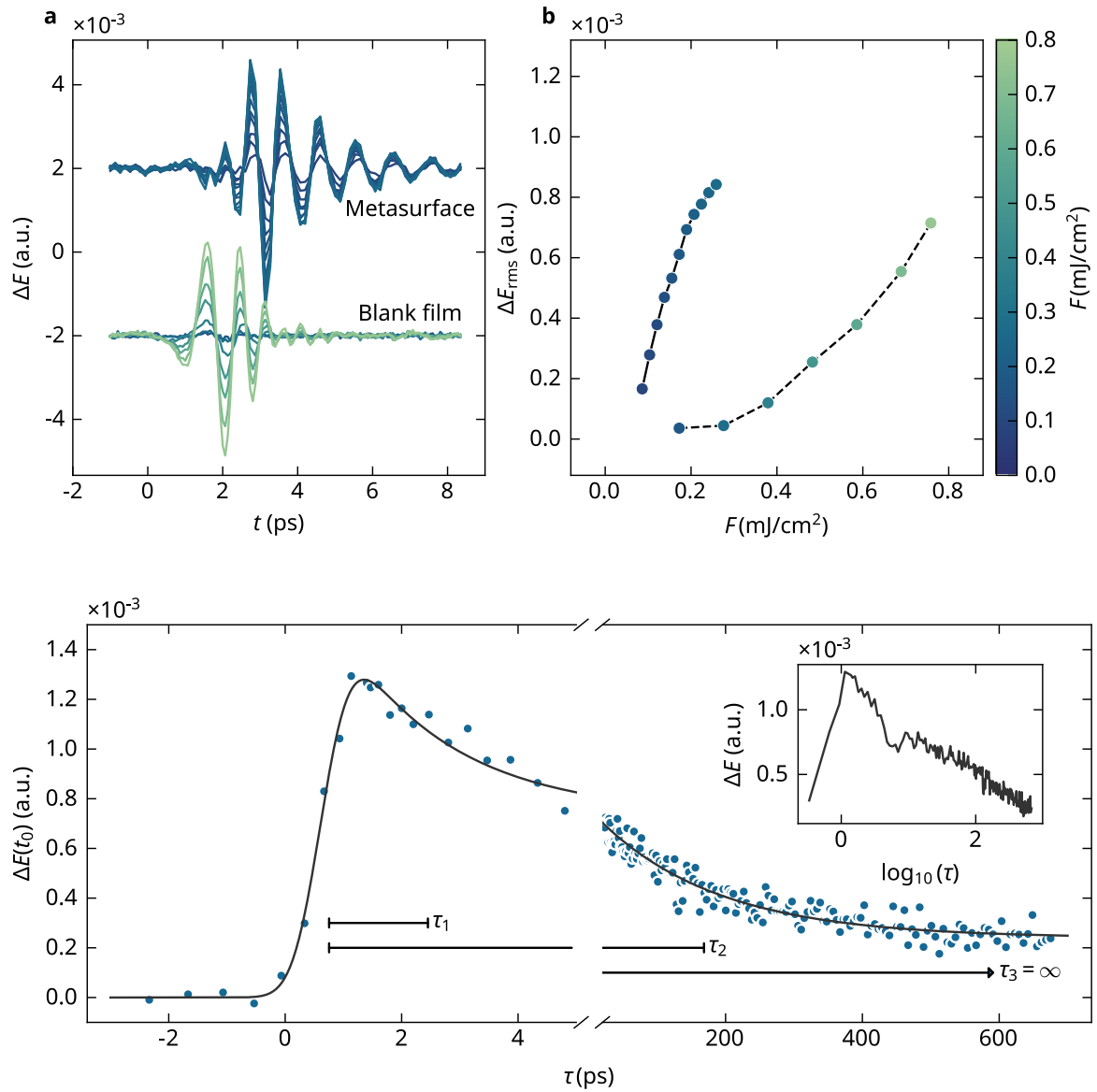


Figure 9.4: Decay times after photoexcitation of the eSRR sample.

# **Part V**

## **Nonlinear spectroscopy**

## 10 Comparing low and moderate temperature

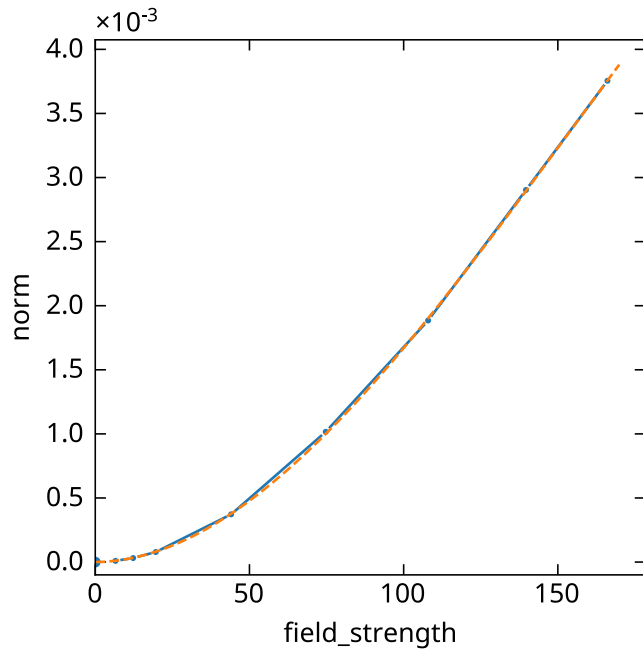


Figure 10.1: The normalization factor (integral of the square of the field) as a function of the field strength, with a polynomial fit pinned to zero.

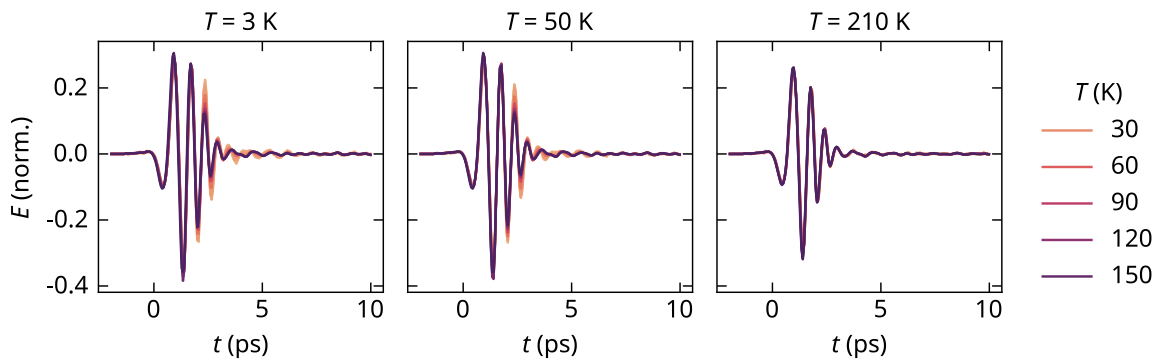
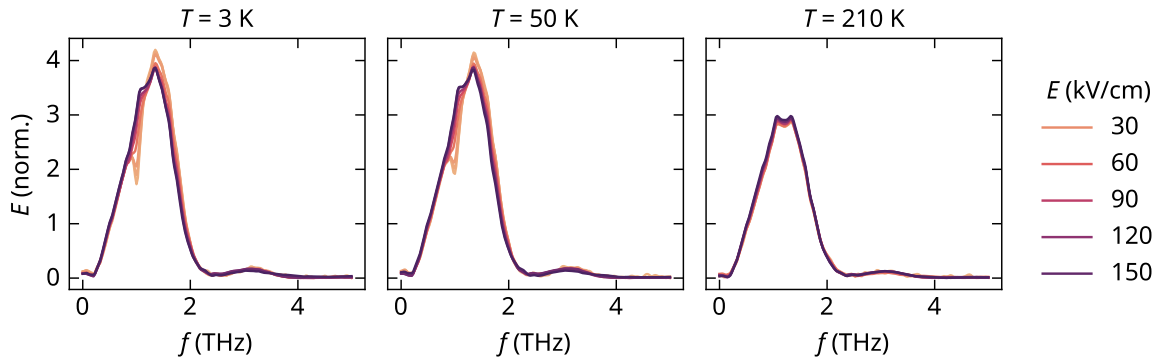
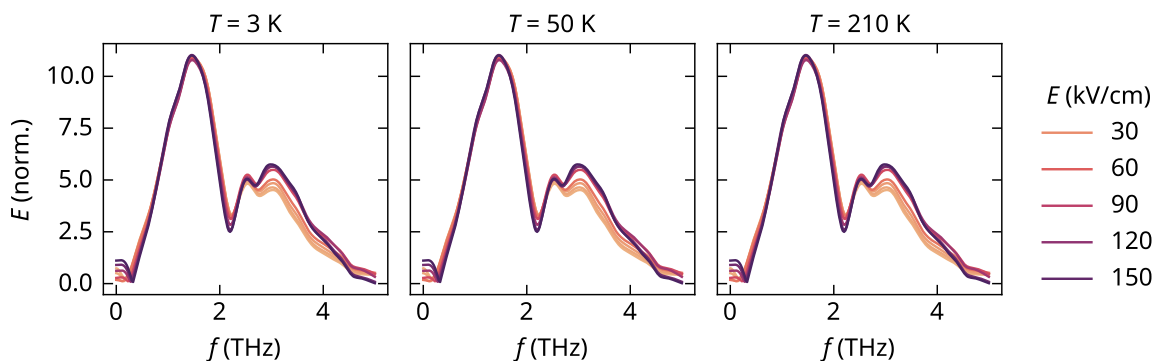


Figure 10.2: Time-domain waveforms at three temperatures, with color representing the relative field strength (1 is about 200 kV/cm incident).



(a) Spectra for waveforms transmitted through sample.



(b) Spectra for waveforms transmitted through vacuum only.

Figure 10.3: Raw spectra of the detected waveforms.

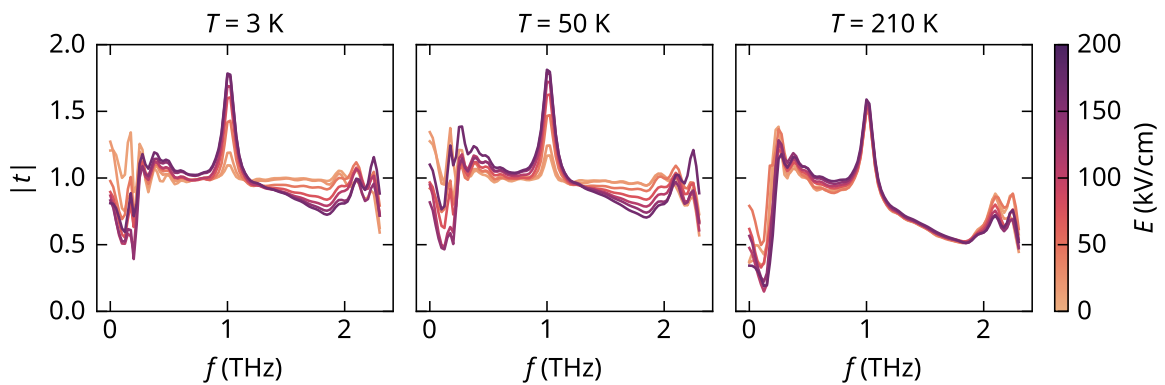


Figure 10.4: Spectra at three temperatures, with color representing the relative field strength (1 is about 200 kV/cm incident).

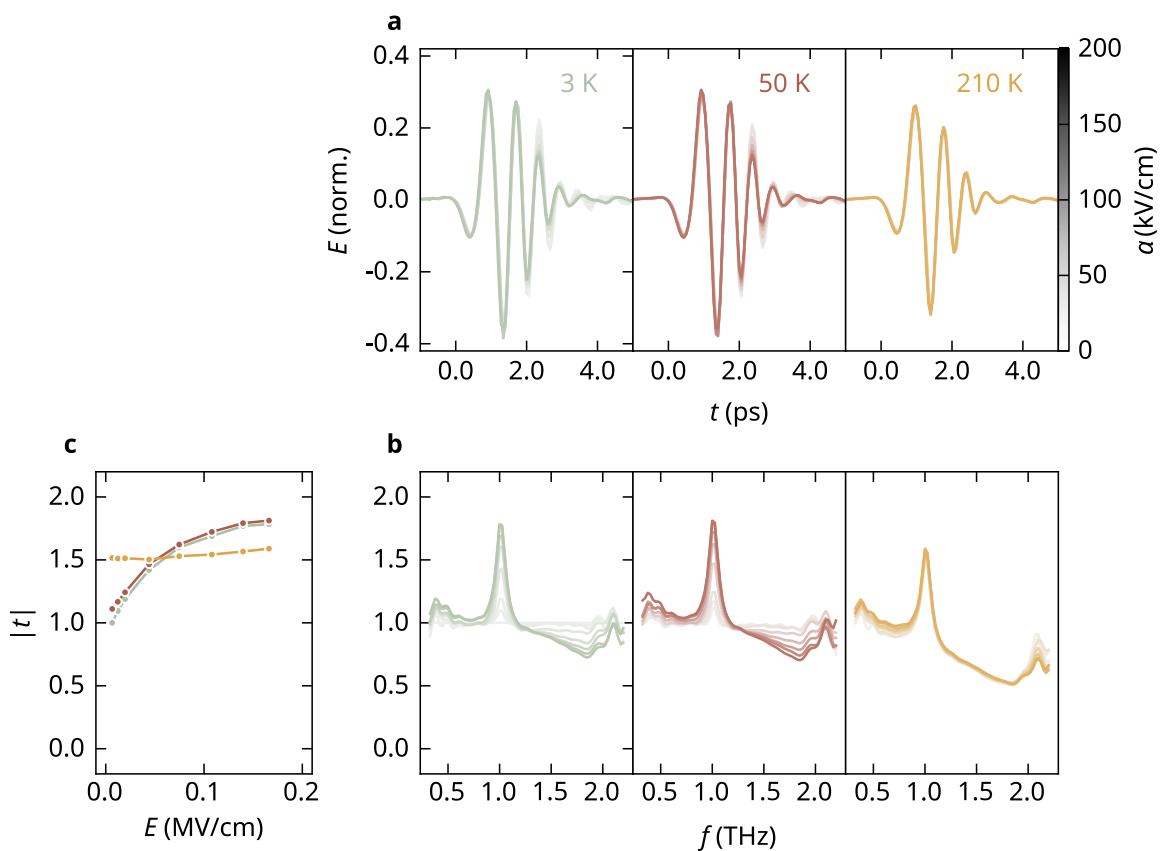


Figure 10.5: Summary of time- and frequency-domain responses at three temperatures, with color representing the relative field strength (1 is about 200 kV/cm incident).

**Part VI**

**Cavity**

# 11 Field enhancement

The fundamental mode of the split-ring resonator involves alternating circulating currents that accumulate charge at the resonator central gap. This charge accumulation produces an evanescent electric field which is larger than the incident electric field. The field enhancement is calculated as

$$|E/E_0| = \left| \frac{E_y(\mathbf{r} = \mathbf{0})}{E_{y,0}(\mathbf{r} = \mathbf{0})} \right|$$

where  $\mathbf{r} = \mathbf{0}$  corresponds to the point at the center of the resonator gap, at the surface. The reference field  $E_{y,0}$  is the field at the same point with the resonator removed.

Table 11.1: Field enhancement data at 1 THz, across the  $xy$ -plane, evaluated at the surface.

x f64	y f64	field_enhancement f64
-25.074	-19.701	0.764352
-25.074	-19.503	0.766842
-25.074	-19.305	0.766758
-25.074	-19.107	0.766634
-25.074	-18.909	0.766544
...	...	...
25.074	18.909	0.766749
25.074	19.107	0.766901
25.074	19.305	0.767095
25.074	19.503	0.767245
25.074	19.701	0.764315

In Figure 11.1, we show the field enhancement at 1 THz, both in the  $xy$ -plane and the profile extending away from the surface.

We have also calculated the surface current distributions,

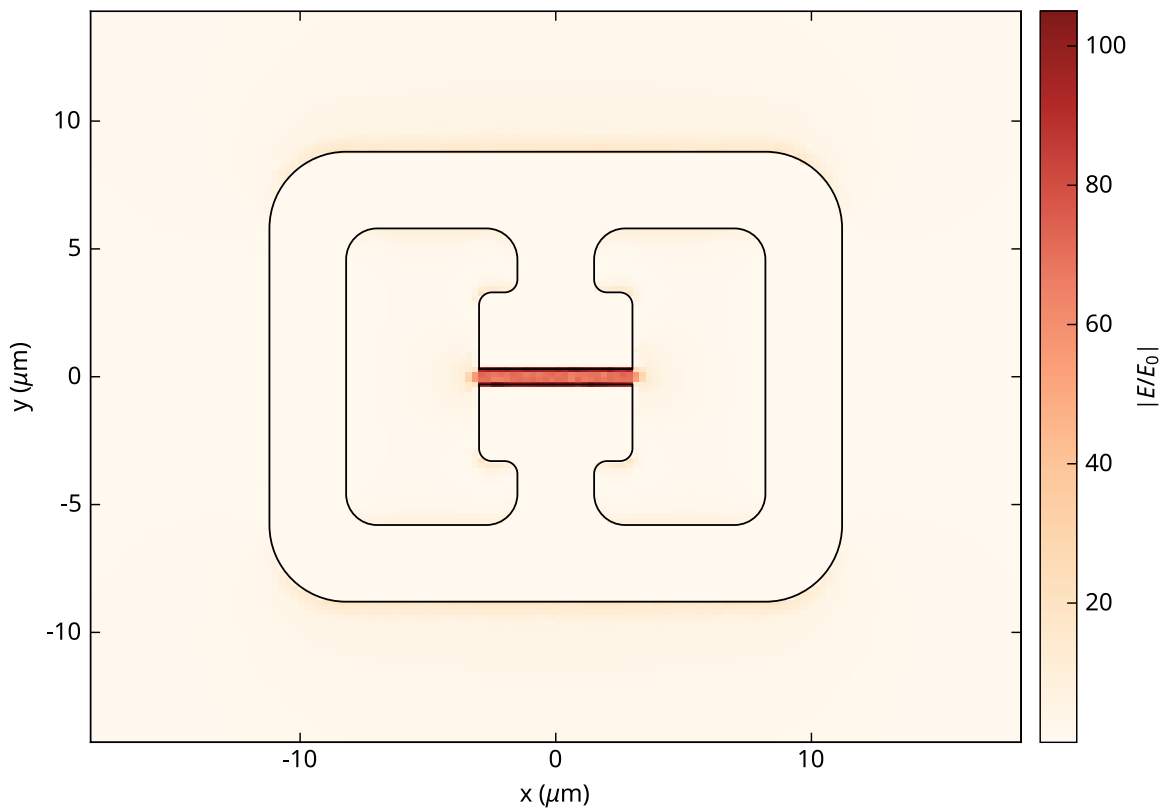


Figure 11.1: Field enhancement at 1 THz, assuming zero conduction in the film.

x f64	y f64	conductivity f64	freq f64	Jx f64	Jy f64
-25.074	-19.701	0.0	1.0	-0.000706	0.000907
-24.822	-19.701	0.0	1.0	-0.000607	-0.000644
-24.57	-19.701	0.0	1.0	-0.000507	-0.001626
-24.318	-19.701	0.0	1.0	-0.000407	-0.002039
-24.066	-19.701	0.0	1.0	-0.000307	-0.001883
...	...	...	...	...	...
24.066	19.701	0.0	1.0	-0.000474	-0.001094
24.318	19.701	0.0	1.0	-0.000567	-0.001115
24.57	19.701	0.0	1.0	-0.000661	-0.000992
24.822	19.701	0.0	1.0	-0.000754	-0.000725
25.074	19.701	0.0	1.0	-0.000848	-0.000314

as well as the perpendicular field distribution. These give a full picture of the cavity mode, and the nature of the field enhancement, summarized in Figure 11.2.

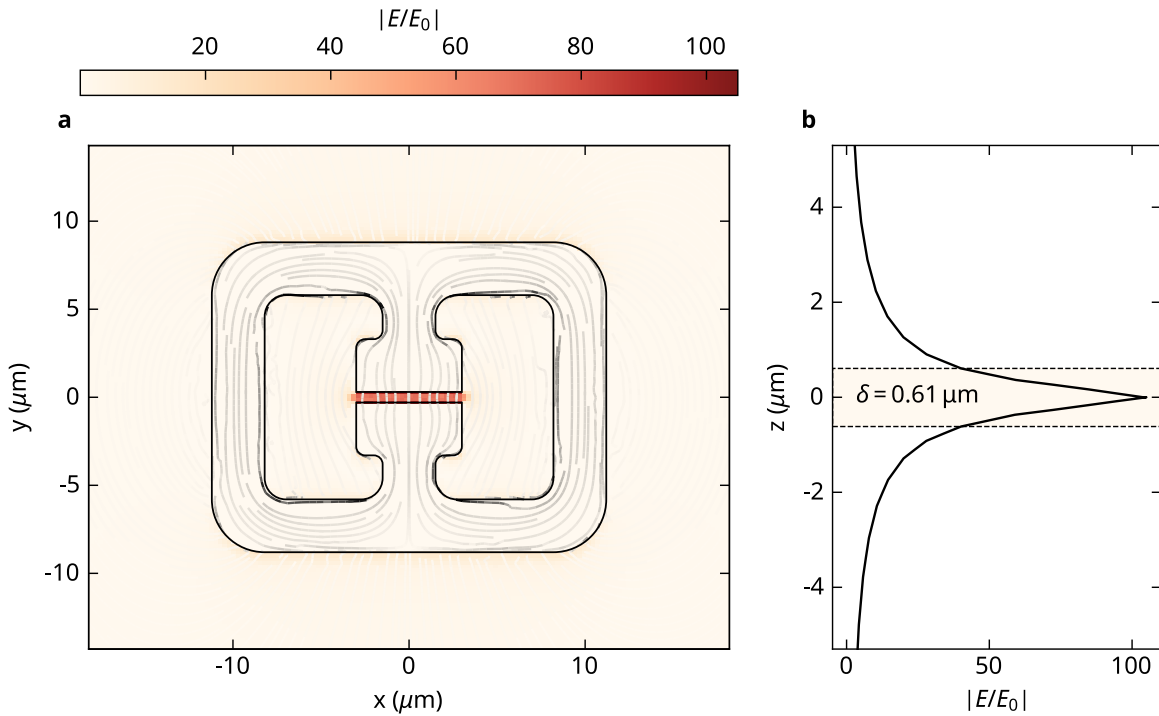
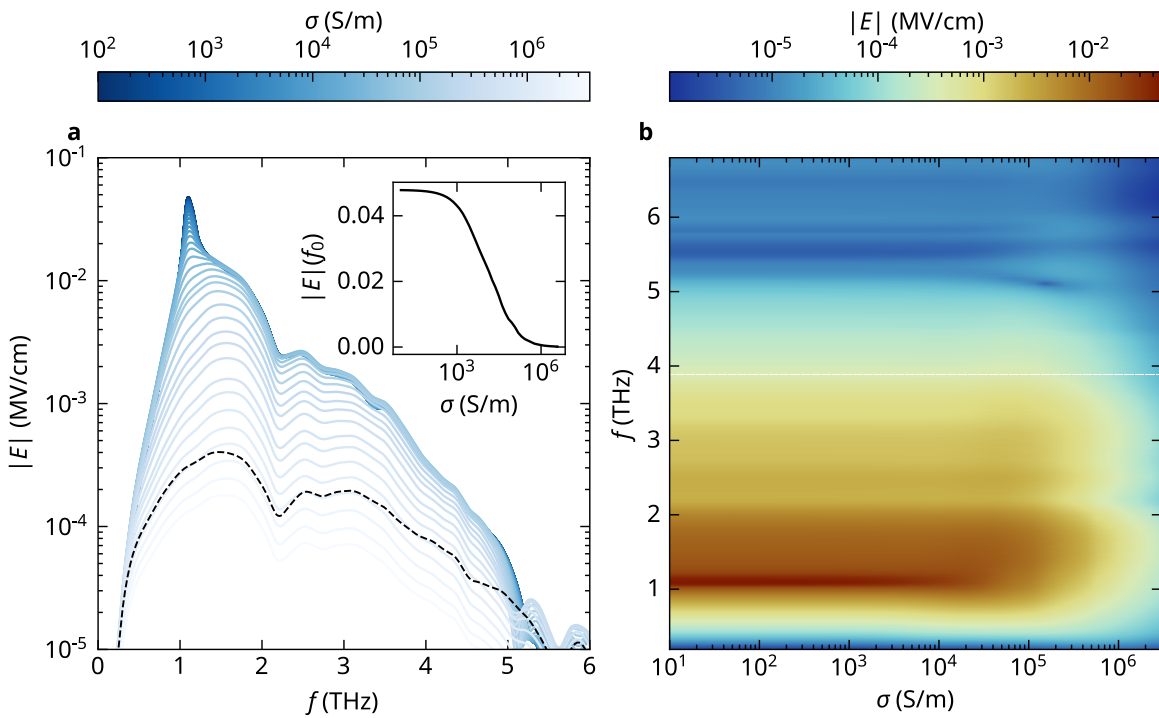


Figure 11.2: Field enhancement at 1 THz, assuming zero conduction in the film.

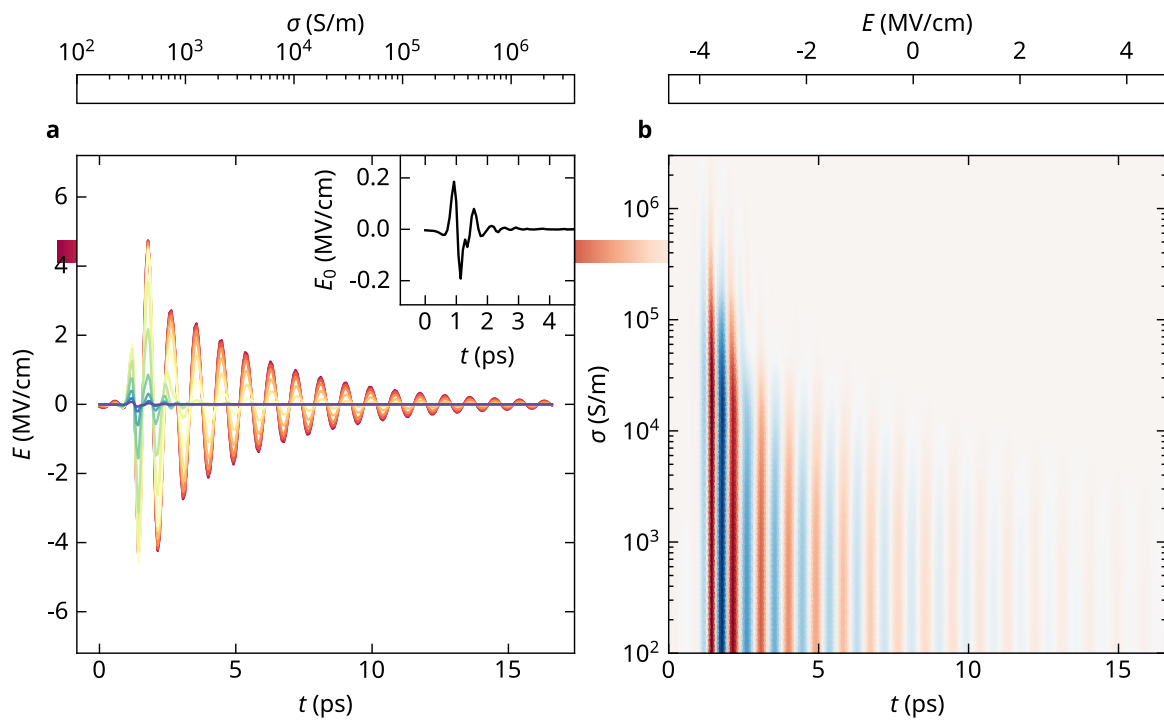
The field enhancement is largest at the center of the resonator gap, and decays rapidly away

from it. The decay length, defined as the distance at which the field enhancement decays to  $1/e$  of its maximum value, is  $\delta = 0.6 \mu\text{m}$ .

cond f64	freq f64	Ey.mag f64	E0y.mag f64
10.0	5.691	663.143904	753.118748
13.070901	5.691	663.143621	753.118748
17.084844	5.691	663.143253	753.118748
22.33143	5.691	663.142766	753.118748
29.18919	5.691	663.142171	753.118748
...	...	...	...
1.3105e6	1.789	57134.612027	33961.924581
1.7130e6	1.789	42305.020321	33961.924581
2.2390e6	1.789	30540.563709	33961.924581
2.9266e6	1.789	21678.41018	33961.924581
3.8253e6	1.789	15710.889106	33961.924581



cond f64	time f64	Ey f64	E0y f64
100.0	0.0	-0.066184	-0.00374
124.594402	0.0	-0.065137	-0.00374
155.237649	0.0	-0.063846	-0.00374
193.41742	0.0	-0.062287	-0.00374
240.987277	0.0	-0.060401	-0.00374
...	...	...	...
1.5920e6	11.182336	-0.00002	-0.000017
1.9835e6	11.182336	-0.000019	-0.000017
2.4713e6	11.182336	-0.000017	-0.000017
3.0791e6	11.182336	-0.000015	-0.000017
3.8364e6	11.182336	-0.000011	-0.000017



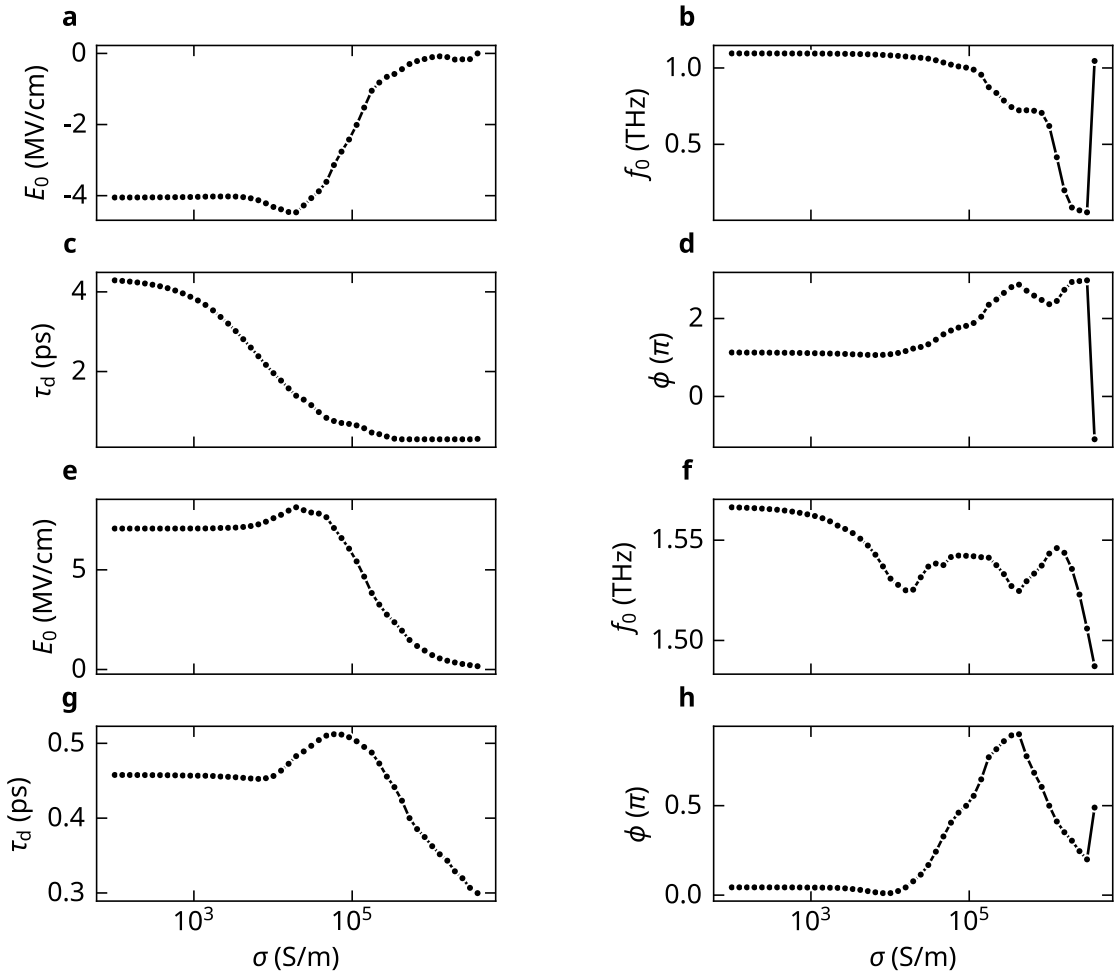


Figure 11.3: Best fit parameters for the temporal field enhancement model. (a-d) First resonance. (e-h) Second resonance.

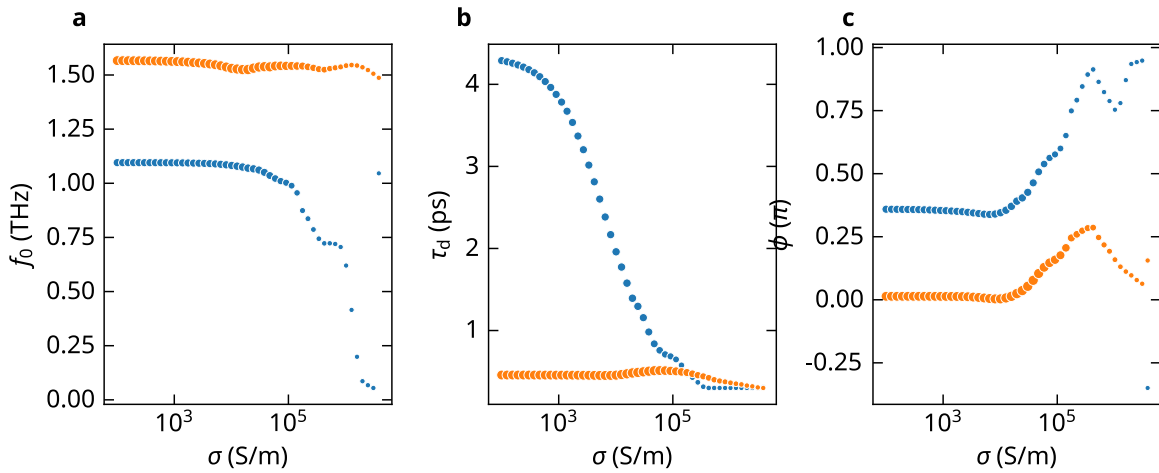


Figure 11.4: Best fit parameters for the temporal dynamics.

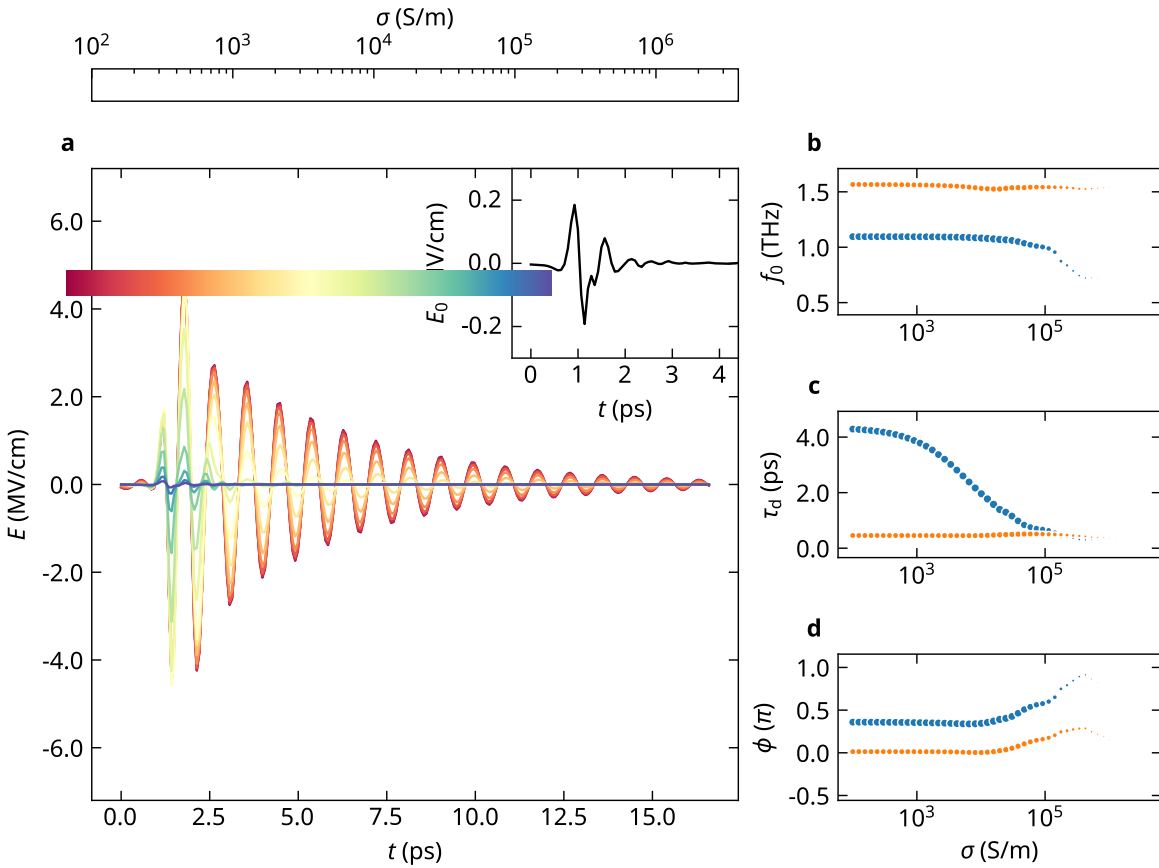


Figure 11.5: Summary of time-domain view.

# 12 Cavity polarization

```
[[Model]]
((Model(sine, prefix='osc_') * Model(exponential, prefix='exp_')) * Model(step, prefix=''))
[[Fit Statistics]]
# fitting method = leastsq
# function evals = 131
# data points = 2666
# variables = 7
chi-square = 1.2479e-05
reduced chi-square = 4.6930e-09
Akaike info crit = -51119.4346
Bayesian info crit = -51078.2162
R-squared = 0.91788095
[[Variables]]
osc_amplitude: 0.00246273 +/- 1579417.89 (64132785369.15%) (init = 0.001)
osc_frequency: 6.47385113 +/- 0.00460220 (0.07%) (init = 6)
osc_shift: -0.59477597 +/- 0.01612088 (2.71%) (init = 0)
exp_amplitude: 1 (fixed)
exp_decay: 2.40825647 +/- 0.03767383 (1.56%) (init = 5)
step_amplitude: 1.16315214 +/- 7.4312e+08 (63888296942.87%) (init = 1)
step_center: 1.92165956 +/- 0.01481390 (0.77%) (init = 0)
step_sigma: 1.76070803 +/- 0.03416195 (1.94%) (init = 2)
[[Correlations]] (unreported correlations are < 0.100)
C(osc_amplitude, step_amplitude) = -1.0000
C(osc_frequency, osc_shift) = -0.9321
C(exp_decay, step_center) = -0.7065
C(step_center, step_sigma) = +0.6396
C(exp_decay, step_sigma) = -0.4354
[[Model]]
((Model(sine, prefix='osc_') * Model(exponential, prefix='exp_')) * Model(step, prefix=''))
[[Fit Statistics]]
# fitting method = leastsq
# function evals = 301
# data points = 2666
# variables = 7
chi-square = 2.2225e-05
```

```

reduced chi-square = 8.3585e-09
Akaike info crit   = -49580.5770
Bayesian info crit = -49539.3586
R-squared           = 0.68608921
[[Variables]]
osc_amplitude:    0.00300960 +/- 3638567.23 (120898739103.85%) (init = 0.001)
osc_frequency:    7.44743514 +/- 0.03280684 (0.44%) (init = 6)
osc_shift:        -0.22963204 +/- 0.04303316 (18.74%) (init = 0)
exp_amplitude:    1 (fixed)
exp_decay:         0.60263743 +/- 0.02580589 (4.28%) (init = 5)
step_amplitude:   2.78520099 +/- 3.3673e+09 (120899340098.18%) (init = 1)
step_center:       1.03397631 +/- 0.04426914 (4.28%) (init = 0)
step_sigma:        1.22396006 +/- 0.07183540 (5.87%) (init = 2)
[[Correlations]] (unreported correlations are < 0.100)
C(osc_amplitude, step_amplitude) = -1.0000
C(osc_frequency, osc_shift)      = -0.9510
C(step_center, step_sigma)       = +0.9343
C(exp_decay, step_center)        = -0.8352
C(exp_decay, step_sigma)         = -0.6595
C(osc_shift, exp_decay)          = -0.2032
C(osc_frequency, exp_decay)      = +0.1986
C(osc_frequency, step_center)    = -0.1823
C(osc_shift, step_center)         = +0.1800
C(osc_frequency, step_sigma)     = -0.1232
C(osc_shift, step_sigma)          = +0.1140

```

